OPTICAL PHASE CONJUGATION VIA STIMULATED BRILLOUIN SCATTERING IN MULTIMODE OPTICAL FIBER

THESIS

Patrick T. Ryan
First Lieutenant, USAF

AFIT/GEP/ENP/90S-1

DEPARTMENT OF THE AIR FORCE
AIR UNIVERSITY
AIR FORCE INSTITUTE OF TECHNOLOGY

Wright-Patterson Air Force Base, Ohio

AFIT/GEP/ENP/90S-1

OPTICAL PHASE CONJUGATION VIA STIMULATED BRILLOUIN SCATTERING IN MULTIMODE OPTICAL FIBER

THESIS

Patrick T. Ryan
First Lieutenant, USAF

AFIT/GEP/ENP/90S-1

AFIT/GEP/ENP/90S-1

OPTICAL PHASE CONJUGATION VIA STIMULATED BRILLOUIN SCATTERING IN MULTIMODE OPTICAL FIBER

THESIS

Presented to the Faculty of the School of Engineering
of the Air Force Institute of Technology
Air University
In Partial Fulfillment of the
Requirements for the Degree of
Master of Science in Engineering Physics

Patrick T. Ryan, B.S.
First Lieutenant, USAF

September, 1990

Acknowledgments

This thesis would not have been viable without the help of many people. Dr. Won Roh provided the technical guidance and handled the hassles of obtaining support for this effort. I am indebted to Captain Jim Targove and Major Steve Rogers for serving on my committee along with Dr. Roh. Karen Wink provided invaluable help as a consultant and in the laboratory. Greg Smith and Leroy Cannon helped obtain equipment and supplied technical knowledge. Dale Stevens, Bob Lindsey and Rick Patton generously supplied advice and essential equipment when my thesis was stalled and Corning donated the optical fiber which I needed. This research was also supported in part by the Air Force Office of Scientific Research and the Air Force Weapons Laboratory.

Finally, I would like to thank my family and friends who supported me emotionally during my studies.

Patrick T. Ryan

Table of Contents

List of Figures

List of Tables

Abstract

The main objective of this thesis was to obtain phase conjugation of an argon-ion laser beam using the process of stimulated Brillouin scattering (SBS) in optical fiber and to characterize the parameters involved. This is of interest because nonlinear optical phase conjugation can compensate for the unavoidable phase distortions which occur in many laser systems. SBS in fiber is an attractive method for generating phase conjugate waves for a number of reasons: a high conversion efficiency, a nanosecond response time, only the signal beam is required and fiber has a lower SBS threshold and superior power handling capabilities compared to either crystals or liquids. SBS theory is briefly described along with some results from previous work.

Experimental results show the multimode fiber losses at coupled powers below about 2 W to be 16.4 $\pm$ 0.3 dB/km at 514.5 nm. The transmitted and backscattered power exhibited behavior similar to that previously reported for single-mode fiber. The SBS threshold power also showed the expected dependences on fiber length and on feedback conditions: the threshold increased for shorter fibers and when index matching liquid was used. The Stokes shift was 32.78 $\pm$ 0.02 GHz and the measured gain was 10.2 $\times$ 10^{-9} cm/W with an error of 10%. Most importantly, nonlinear optical phase conjugation was demonstrated for the first time. Aberrations introduced by a phase plate placed in the optical path were compensated upon retraversal of the plate by the SBS beam. The polarization state of the pump beam was not reproduced, however. In addition, the SBS power exhibited bursts of strong fluctuations, in some cases with up to 100% modulation.

OPTICAL PHASE CONJUGATION VIA STIMULATED BRILLOUIN SCATTERING IN MULTIMODE OPTICAL FIBER

I. Introduction

All optical beams suffer degradations due to atmospheric turbulence as they propagate. Optical phase conjugation is capable of eliminating phase distortions on a wavefront by reversing the direction of propagation and the overall phase factor of the wave. Figure 1 illustrates this effect. Initially, the wave travels to the right and is distorted upon passing through the spatially-varying phase delays of the aberrator. The phase conjugator performs a complex conjugation on the spatial portion of the wave so that it retraverses the aberrator. The distortions on the wavefront are cancelled by the phase delays in the aberrator and the original wavefront is restored. An ordinary mirror merely reflects the distorted wavefront, which compounds the distortions upon retraversal of the aberrator. Phase conjugation will only eliminate distortions if the same phase delays are present for the second pass as for the first. Thus, the phase conjugation must occur with a faster response time than the time it takes for the distortions to change.

The requirement for a fast response time is the fundamental limiting factor of mechanical phase conjugation. However, it has the advantage of conjugating weak signal beams and is used, with some success, since all other methods of phase conjugation have limitations also. Four-wave mixing has a fast response time and succeeds with a weak signal, but two strong pump beams are required in addition to the signal beam. Stimulated Raman scattering has had little success due to the large frequency shift of the Stokes beam. Stimulated Brillouin scattering (SBS) has

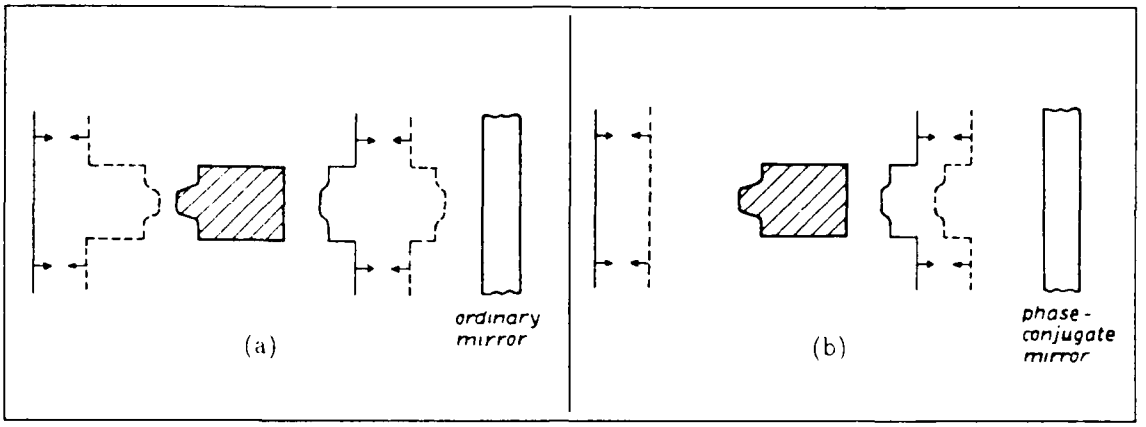

Figure 1. Illustration of the restoration of a wavefront by phase conjugation. (a) ordinary mirror, (b) phase-conjugate mirror

nanosecond response times and a small frequency shift but, in a focused geometry configuration, it requires a high intensity signal.

The strength of the SBS process scales with the intensity of the pump beam and the length of the interaction region. Waveguides have been used in an attempt to extend the interaction length without lowering the intensity. This has reduced the power requirements to some degree, but the length is still generally only a few meters when using cells. In addition, cells are bulky and fragile. Using optical fiber extends the interaction region into the kilometer range and further increases the beam intensity at the cost of increased focusing requirements. The enhancement of the intensity and interaction length more than compensate for fiber, made of silica, having a lower nonlinear optical susceptibility than other materials which can only be used in bulk. Additionally, silica fiber has low losses and superior power handling capabilities compared to nonlinear crystals and liquids. Thus, optical phase conjugation via stimulated Brillouin scattering in multimode optical fiber seems to offer the possibility of a fast and easy way to correct phase aberrations in laser beams.

This thesis begins in Chapter II with some background material concerning fiber as a medium for light transmission. Chapter III gives a basic description of the theory describing SBS. A review of the results of the previous work in this area is sketched in Chapter IV. Experimental results are presented and analyzed in Chapter V. Finally, Chapter VI summarizes the findings as they relate to possible further work in this area.

II. Optical Fiber

In order to use optical fiber to generate stimulated Brillouin scattering, a basic understanding of how fiber confines light, how light can be coupled into fiber and the fiber parameters pertinent to nonlinear effects is needed. This chapter discusses these topics.

Optical fiber consist of three concentric sections: (1) a central core which propagates most of the light, (2) a cladding which helps confine the light to the core and (3) a coating which protects the core and cladding. Energy is confined in a small area, the core, for long distances by an index of refraction which gradually decreases radially, usually parabolically, (graded-index fiber) or decreases rapidly in a step function at the core-cladding interface (step-index fiber). In a graded-index fiber, when the light strays outward, it bends back toward the center of the fiber because the light is traveling slower there than further out in the cladding. In a step-index fiber, light totally internally reflects at the core-cladding interface due to the abrupt difference in refractive index and the large angle of incidence.

In order to efficiently couple light into either kind of fiber two conditions must be fulfilled. First, the input beam must be focused so that its diameter is less than the core diameter of the fiber. At the same time, once inside the fiber, the light must propagate with a small enough angle to the fiber axis so as to be confined by the refractive index difference. This requirement is satisfied if the light hits the fiber at an angle θ_{inc} such that

$$\theta_{inc} \leq \sin^{-1}(NA) \tag{1}$$

where NA, the numerical aperture, is defined as

$$NA = (n_{core}^2 - n_{cladding}^2)^{1/2} \tag{2}$$

Here n is the refractive index of the core or cladding. Light entering the fiber at larger angles rapidly dissipates through the cladding. These two criteria impose contrasting restrictions on the focal length of the lens used to focus the light into the fiber. The spot size restriction imposes an upper limit on the focal length

$$f \leq \frac{d_{fiber} \pi d_{beam}}{4\lambda} \tag{3}$$

while the angle restriction imposes a lower limit

$$f \geq \frac{d_{beam}}{2\tan[\sin^{-1}(NA)]} \approx \frac{d_{beam}}{2NA} \tag{4}$$

where f is the focal length of the lens, λ is the light's wavelength, d_{beam} is the beam diameter at the lens and d_{fiber} is the fiber core diameter. The focal lengths which fit this range for the fiber used here were 6–19 mm.

Coupling efficiency C_o decreases if the above conditions are not met, if the fiber is out of alignment or if the fiber end is badly cleaved or dirty. Appendix A details the alignment procedures used in this thesis. Coupling efficiency is measured by calculating the percentage of incident power which passes through the lens and a two meter long fiber. Two meter lengths are used because they are short enough that the fiber losses are usually negligible but long enough so that most of the light coupled into the radiative modes of the fiber has already exited through the sides.

Once the light is confined by the fiber, the properties of the fiber influence how the light behaves. Many of these properties can be determined from a few commonly used parameters. The numerical aperture has already been introduced, but it can also be defined in terms of the fractional refractive index difference Δ by

$$NA = n_{core}(2\Delta)^{1/2} \tag{5}$$

where

$$\Delta = \frac{n_{core}^2 - n_{cladding}^2}{2n_{core}^2} \tag{6}$$

The so-called V value is the most important fiber parameter because it contains several other parameters. It is defined by:

$$V = \frac{4\pi d_{fiber}}{\lambda}(n_{core}^2 - n_{cladding}^2)^{1/2} = \frac{4\pi d_{fiber}}{\lambda} NA \tag{7}$$

The V value is sometimes referred to as the normalized frequency, although it is a structural parameter rather than a frequency. The number of guided modes N_m supported in a step-index fiber can be found from the V value using

$$N_m = V^2/2 \tag{8}$$

Thus the number of modes varies quadratically with the light's wavelength and the fiber's core diameter.

An obvious fiber parameter is the length. However, this is frequently adjusted before being used in SBS calculations for the following reason. As light travels down a fiber it experiences losses due to such things as fiber bending, cation-oxygen and hydroxide absorption, and Rayleigh scattering. The important losses at 514.5 nm are bending and Rayleigh scattering. Bending losses can be minimized by simply not allowing the radius of curvature of the fiber to be less than a few centimeters. However, once a fiber is manufactured, only changing the light's wavelength can change the Rayleigh losses. To compensate for the varying intensity levels along the fiber due to these losses, an effective length L_{eff} is commonly used in the nonlinear equations. It is defined by

$$L_{eff} = [1 - \exp(-\alpha L)]/\alpha \tag{9}$$

where α is the fiber loss coefficient and L is the fiber length. Using the effective length in place of the actual fiber length simplifies many calculations.

Although the loss coefficient α is usually used in equations with units of cm^{-1}, it is usually stated as K in units of dB/km. The two are related by

$$\alpha = 0.2303 \times 10^{-5} K \tag{10}$$

The final parameter to be used here is the effective core area A_{eff}, the area in which energy is concentrated. In the general case, this differs from the actual core area because energy in a fiber is not uniformly distributed over the core; different fiber modes have peak intensities at different spatial locations. For the lowest order mode the light is centrally peaked with about 20% of the energy being outside the core. However, for higher order modes the intensity has peaks at various locations within the core and practically no energy exists outside the core. For multimode fibers, if most of the available modes are excited, then the spatial intensity distribution is approximately level over the core and zero in the cladding. Thus, given some restrictions, the actual core area is a good approximation to the effective core area and is commonly used(1).

III. SBS Theory

3.1 Fundamentals of SBS

Stimulated Brillouin Scattering (SBS) consists of a strong, coherent light wave interacting in a nonlinear medium with acoustic waves to produce a frequency down-shifted scattered light wave, known as the Stokes wave. The process will be considered both classically and quantum mechanically.

The classical description makes a number of approximations (2:26–29, 34–37):

- The medium response is local via the electric-dipole approximation
- The nonlinear response of the medium is much less than the linear response
- Because losses are small, the imaginary part of the dielectric constant ϵ is negligible compared to the real part so that $\epsilon(\omega) \simeq n^2(\omega)$ where $n(\omega)$ is the linear part of the refractive index
- Because $n(\omega)$ is independent of the spatial coordinates in both the core and the cladding of step-index fibers, $\epsilon \vec{\nabla} \cdot \vec{E} = 0$ so that $\vec{\nabla} \times \vec{\nabla} \times \vec{E} = -\vec{\nabla}^2 \vec{E}$ where $\vec{E}$ is the electric field
- All waves are quasi-monochromatic
- Medium response is instantaneous
- All waves have a slowly varying amplitude compared to the optical period
- The electric field is linearly polarized over the interaction region

The last approximation is not true in multimode fiber, but dropping it would only add more terms similar to the ones which are retained and would not change this basic description of SBS.

Initially the only wave present is the pump wave, whose direction of propagation will be called the forward direction. The Stokes wave is generated by the pump wave scattering off of thermal fluctuations in the medium, which can be viewed as an

elastic continuum. The electric field produced by the pump and Stokes waves creates an electrostrictive force which is linearly dependent upon $\frac{\partial}{\partial x_i}(E_j\,E_k)$ where x_i is the unit vector in the i^{th} spatial direction and E_j and E_k are the electric fields in the j^{th} and k^{th} directions, respectively. If the Stokes wave's frequency and direction are right, the interference of the Stokes' and pump's electric fields produce a disturbance whose speed, $d(\Delta\omega)/d(\Delta k)$, matches that of elastic waves. The terms Δk and $\Delta\omega$ are the differences between the two waves' wavevectors and angular frequencies, respectively. The elastic waves are excited and modulate the optical susceptibility of the medium by the photoelastic effect. This in turn modulates the nonlinear part of the dielectric constant $\epsilon_{\rm NL}$ according to

$$\epsilon_{\rm NL} = \frac{3}{4}\,\chi^{(3)}_{xxxx}\,|E(r,t)|^2 \tag{11}$$

where $\chi^{(3)}$ is the third order optical susceptibility tensor. The interaction of the modulated dielectric constant and the optical waves creates a polarization current whose nonlinear term

$$P_{NL}(r,t) = \epsilon_\circ\,\epsilon_{\rm NL}\,E(r,t) \tag{12}$$

serves as a source for the Stokes wave in

$$\nabla^2 E - \frac{1}{c^2}\frac{\partial^2 E}{\partial t^2} = -\mu_\circ\frac{\partial^2 P_L}{\partial t^2} - \mu_\circ\frac{\partial^2 P_{NL}}{\partial t^2} \tag{13}$$

Here P_L is the linear component of the polarization, c is the speed of light, t is time, $\mu_\circ$ is the vacuum permeability and $\epsilon_\circ$ is the vacuum permittivity (3, 2:26–29,34–37).

A slightly different viewpoint is that the interaction of the pump and Stokes waves creates a modulation in the index of refraction $\bar{n}$ given by

$$\bar{n}(\omega,|E|^2) = n(\omega) + n_2\,I \tag{14}$$

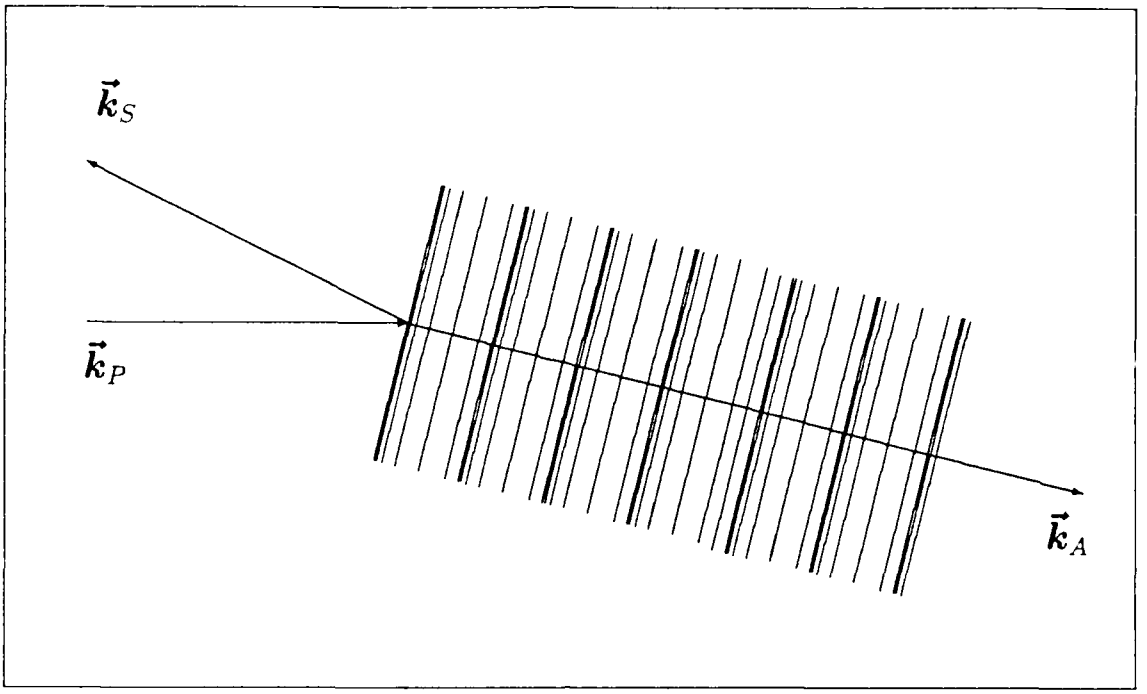

Figure 2. Illustration of the diffraction of light by an acoustic wave. $\vec{k}_P$, $\vec{k}_S$ and $\vec{k}_A$ refer to the pump, Stokes and acoustic wavevectors, respectively.

where I is the optical intensity and n_2 is the nonlinear-index coefficient related to the third order optical susceptibility by

$$n_2 = \frac{3}{8\,n(\omega)}\chi^{(3)}_{xxxx} \tag{15}$$

The Stokes wave grows due to the pump wave Bragg scattering off of the grating made in the index of refraction. This is illustrated in Figure 2. The Stokes wave is frequency downshifted because the grating is moving in the forward direction due to the waves' frequency difference (2:34–37).

These explanations show the relative importance of the different orders of the optical susceptibility. $\chi^{(1)}$ is dominant and accounts for the linear term in Eq 14, $n(\omega)$. However, it is constant over the medium, so it does not generate any backre-

flection. $\chi^{(2)}$ is neglible because the fiber (made of SiO_2) is nearly centrosymmetric (2:290). The most important susceptibility term for SBS is $\chi^{(3)}$; it is directly responsible for the backscattered wave. Terms higher than third order are progressively smaller.

A quantum mechanical viewpoint also starts with the pump being the only light wave in the medium and thermal fluctuations being present. The pump wave spontaneously scatters off of these fluctuations (acoustic phonons) producing weak optical waves. With an assumption of steady state operation, the (continuous) wave which is traveling opposite to the direction of propagation of the pump wave , and thus continuing to interact with it, will grow in a manner similiar to stimulated emission:

$$\frac{d\,I_S}{dz} = -g_B\,I_P\,I_S + \alpha I_S, \tag{16}$$

$$\frac{d\,I_P}{dz} = -g_B\,I_P\,I_S - \alpha I_P \tag{17}$$

where the subscripts P and S refer to the pump wave and the stimulated wave, respectively, I is the wave intensity, g_B is the Brillouin gain, z is the axial spatial coordinate and α, the fiber loss, is taken to be the same for both waves despite the slight frequency difference. An acoustic wave grows along with the Stokes wave at the expense of the pump. However the acoustic wave is strongly damped with a lifetime on the order of 10^{-8} seconds, so its growth equation is not necessary for this development. Notice that when there is no fiber loss ($\alpha = 0$),

$$\frac{d}{dz}(I_S - I_P) = 0, \tag{18}$$

as it should to conserve energy (2:268).

Conservation of energy and momentum requires

$$\omega_A = \omega_P - \omega_S \tag{19}$$

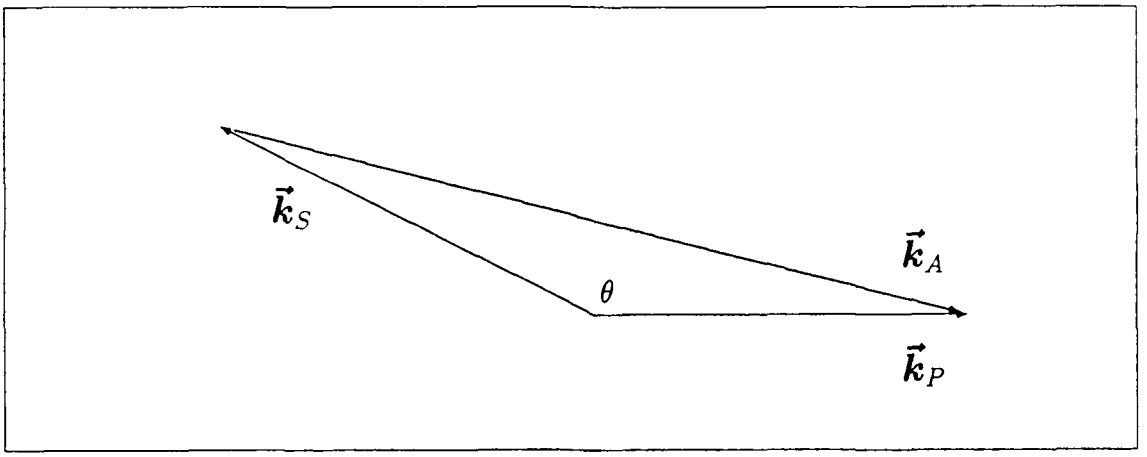

Figure 3. Illustration of the conservation of momentum in SBS. Note that the pump and Stokes momentums have approximately equal amplitudes.

$$\vec{k}_A = \vec{k}_P - \vec{k}_S \tag{20}$$

Here ω and $\vec{k}$ are the angular frequency and the wave vector, respectively. The subscript A refers to the acoustic wave. Because the acoustic wave has a much smaller frequency than the other waves, the pump wave and stimulated wave have nearly the same magnitude wave vectors, as illustrated in Figure 3. Thus Eqs 19 and 20 result in the dispersion relation:

$$\omega_A = |\vec{k}_A|\, V_A = 2\, V_A\ |\vec{k}_P| \sin(\theta/2) \tag{21}$$

where V_A is the acoustic wave's velocity and θ is the angle between the pump and Stokes waves (2).

In fibers the only relevant directions are approximately forward and backward. In the forward direction, $\theta = 0$, there is no frequency shift. This case will be ignored since no SBS occurs. For the backward case, $\theta = \pi$, the Stokes shift, which is the

same as the acoustic frequency ν_A, is maximum:

$$v_A = \omega_A/(2\pi) = 2\,n(\omega)\,V_A/\lambda_P \tag{22}$$

where λ_P is the pump's wavelength. For bulk silica the acoustic velocity is 5.96×10^5 cm/sec and the refractive index is about 1.46, which gives a theoretical shift of 33.8 GHz at 514.5 nm. Approximate shifts can be found from

$$v_A = 17/\lambda_P \tag{23}$$

where the shift is given in gigahertz if the wavelength is given in micrometers (4). The shift has been shown to be slightly affected in fibers with core diameters of 3 μm or less due to the effects of the finite geometry on the acoustic mode spectrum and the acousto-optic interactions (5, 6).

The only shifts which will be amplified are those which fall within the gain spectrum of the material; therefore, the shifts for which the material supports acoustic waves. If the acoustic waves are assumed to decay as exp(-t/T_B) with t being time and T_B being acoustic lifetime, the Brillouin gain $g_B(\nu)$ has a Lorentzian spectral profile given by

$$g_B(\nu) = \frac{(\frac{\Delta\nu_B}{2})^2}{(\nu - \nu_B)^2 + (\frac{\Delta\nu_B}{2})^2} g_B(\nu_B), \tag{24}$$

where ν is the Stokes frequency, $g_B(\nu_B)$ is the gain at the shift given by Eq 22 and $\Delta\nu_B$, the gain bandwidth, is related to the phonon lifetime by $\Delta\nu_B = (\pi\,T_B)^{-1}$. The commonly accepted value for bulk silica is 145 MHz at 514.5 nm (4). However, Thomas *et al.* have proven theoretically that in small core diameter fibers the finite geometry effects can widen the bandwidth by up to 25%, to 178 MHz (6, 5).

The peak value of the Brillouin-gain coefficient occurring at $\nu = \nu_B$ is given by

$$g_B(\nu_B) = \frac{2\,\pi\,n^7\,p_{12}^2}{c\,\lambda_P^2\,\rho_0\,v_B\,\Delta\nu_B} \tag{25}$$

where p_{12} is the longitudinal elasto-optic coefficient and ρ_0 is the material density (7). The theoretical peak gain for fused silica is 5×10^{-9} cm/W. The gain bandwidth dependence on wavelength

$$\Delta\nu_B \propto \lambda^{-2} \tag{26}$$

approximately cancels the apparent decrease in peak gain in Eq 25 (1, 8). Consequently the peak gain is largely independent of the wavelength (2). The actual gain $\tilde{g}_B(\nu)$ is substantially lowered if the spectral width of the pump beam $\Delta\nu_P$ is larger than the gain bandwidth (9, 10, 11, 12). If the pump has a Lorenzian bandwidth, the actual gain is given by (11)

$$\tilde{g}_B(\nu) = \frac{\Delta\nu_B}{\Delta\nu_B + \Delta\nu_P} g_B(\nu) \tag{27}$$

3.2 SBS Solution Without Pump Depletion

A simplified equation representing the Stokes wave can be found by neglecting pump depletion. The Stokes intensity then grows exponentially in the backward direction (2):

$$I_S(0) = I_S(L)\, \exp(\tilde{g}_B(\nu)\, P_0\, L_{eff}/A_{eff} - \alpha\, L) \tag{28}$$

where $P_0 = I_P(0)\, A_{eff}$, $I_P(0)$ is the pump intensity at the input end of the fiber, $I_S(L)$ is the injected Stokes intensity at the far end of the fiber, A_{eff} is the effective area, L_{eff} is the effective fiber length and L is the actual fiber length. This assumes that the Stokes wave is injected. If a Stokes wave is not injected, then it will grow from noise due to spontaneous Brillouin scattering. In this case, this is equivalent to injecting a fictitious photon per mode at a distance where the gain equals the fiber loss (13).

The exponential growth along the interaction region causes the shift corresponding to the peak gain ν_B to dominate the return. The higher the pump power is, the more ν_B dominates the SBS and the narrower the bandwidth of the SBS is.

An approximate value for the Brillouin threshold can be found for long low-loss fibers using

$$\tilde{g}_B(\nu)\, P_{threshold}\, L_{eff}/A_{eff} \approx 21 \tag{29}$$

where $P_{threshold}$ is the threshold pump power (13). The 21 varies depending on whether the pump and Stokes waves maintain their polarization along the fiber or not. For completely scrambled polarization, the 21 doubles (1, 2:268–269).

Eq 29 shows that the SBS threshold decreases as the fiber length increases. In addition, the Fresnel reflections at the fiber end faces tend to reduce the threshold because more laser energy will be available inside the fiber and the Stokes beam can be further amplified without having to input more energy (4, 14). When an optical resonator is formed by the fiber end faces, the SBS threshold power is given by

$$R_{input}\, R_{fa\text{-}}\, \exp(-\alpha\, L) \exp(\tilde{g}_B\, P_{threshold}\, L_{eff}/A_{eff}) = 1 \tag{30}$$

where R is the reflectivity at the input and far ends of the fiber (4).

3.3 SBS Solution Including Pump Depletion

Equations for the pump and Stokes intensities including pump depletion and gain saturation were given by Tang as

$$I_S(z) = \frac{b_0\,(1-b_0)}{G(z)-b_0}\, I_P(0)\, \exp(-\alpha\, z) \tag{31}$$

$$I_P(z) = \frac{G(z)\,(1-b_0)}{G(z)-b_0}\, I_P(0)\, \exp(-\alpha\, z) \tag{32}$$

where

$$G(z) = \exp\{g_0\,(1-b_0)\,[1-\exp(-\alpha\, z)]/\alpha\}$$

$$b_0 = \frac{I_S(0)}{I_P(0)}$$

$$g_0 = \tilde{g}_B(\nu)\, I_P(0)$$

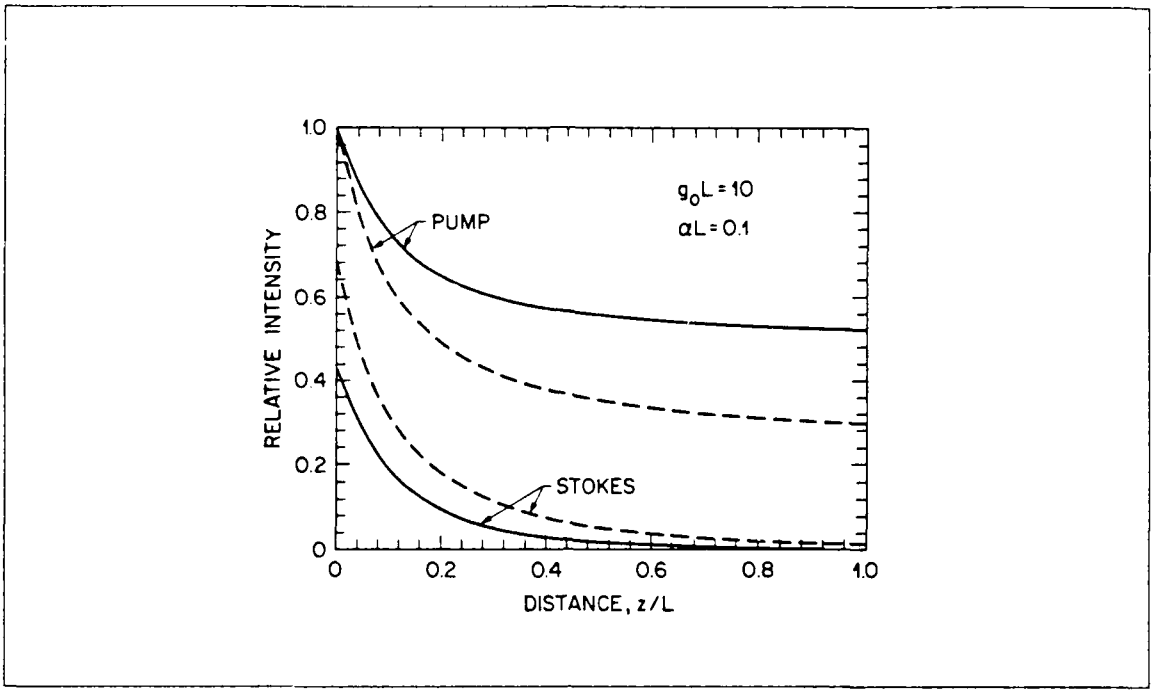

Figure 4. Relative intensity variation (normalized to the input pump intensity) of the pump and the Stokes beams along the fiber length for a relative input intensity (at z = L) of 0.001 (solid lines) and 0.01 (dashed lines). From Agrawal, reference (2:27).

The parameter b_0 is a measure of the Brillouin efficiency, the fraction of the pump power which is converted to Stokes power. The parameter g_0 is the small-signal gain associated with the SBS process (7). Figure 4 illustrates these equations.

3.4 SBS Power Fluctuations

The development so far has been for steady state conditions. However, Johnson and Marburger (15) and Bar-Joseph *et al.* (16) have reported that reflections back into the medium can cause fluctuations in the SBS power with periods equal to the round trip time of light in the medium or its harmonics. These fluctuations are due to changing depletion rates in the pump wave at different positions along the fiber.

When SBS power is high near the input end of the fiber, a lot of the pump wave is converted to SBS there, which leaves only a weak pump wave to propagate further into the fiber. Since the pump wave which survives far into the fiber is weak, little SBS is created there and a weak SBS wave travels back towards the input end. When the weak SBS reaches the input end, the strong SBS which was there has already left the fiber. This means that a lot of pump power can now propagate far into the fiber to create a lot of SBS there. This strong SBS propagates back to the input end and the cycle starts over again.

Aside from these fluctuations, the SBS in fiber can be chaotic as recently shown by Lu and Harrison (17). They included the self and cross phase modulation terms, which are usually dropped, in the general coupled first order nonlinear partial differential equations. These terms, which arise from the nonlinear dispersion, lead to changes in both the pump and Stokes fields in space and time.

3.5 Phase Conjugating Properties of SBS

The phase conjugate nature of the stimulated wave occurs because the gain is higher for a phase-conjugate wave than for a non-conjugate wave. The effective gain can be written (18)

$$g_{eff} = \frac{\int \tilde{g}_B(\nu)\ |E_P(\boldsymbol{r},z)|^2\ |E_S(\boldsymbol{r},z)|^2\ d^2\boldsymbol{r}}{\int\ |E_S(\boldsymbol{r},z)|^2\ d^2\boldsymbol{r}} \tag{33}$$

Therefore, maximum gain is achieved for a wave whose local intensity maxima coincide everywhere in space with the maxima of the pump wave E_P. To maintain the correlation of two fields throughout the interaction volume, the generated field $E_S(\boldsymbol{r},z)$ must be the conjugate of $E_P(\boldsymbol{r},z)$. Thus the wave with the highest correlation over the interaction region, the phase conjugate, will have the greatest gain and dominate due to the exponential growth (19):

$$E_S(\boldsymbol{r},z) \sim E_P^*(\boldsymbol{r},z) \tag{34}$$

IV. Previous Experimental Results

Phase conjugation via SBS in multimode waveguides was first reported by Zel'dovich *et al.* in early 1972 (20). The fidelity was measured at 100% with a 15% error. Wang and Giuliano (21), Lind and Giuliano (22) and Mays and Lysiak (23, 24) have all quantitatively investigated parameters of phase conjugation in waveguides and found greater than 90% fidelity.

In late 1972, Ippen and Stolen observed SBS in an single-mode optical fiber for the first time (25). Figure 5 is a sketch of the experimental setup. They used a pulsed xenon laser, $\lambda = 535.5$ nm, to generate the pump beam. The measured gain was 4.6×10^{-9} cm/W and the frequency shift was 32.2 GHz, in agreement with the theoretical value predicted by Eq 22.

Continuous wave SBS was initially generated by Hill *et al.* using a ring-cavity configuration (26). This lowered the threshold power and converted greater than 40% of the power to the Stokes line. They also used a Fabry-Perot fiber resonator setup to generate multiple continuous wave SBS peaks (27). Lowering the threshold through feedback has also been reported by Labudde *et al.* (4), Boyd *et al.* (28) and Wong and Damzen (14) as well.

Polarization effects were investigated in 1979 by Stolen using birefringent fiber (29). He verified the factor of two difference in the gain between when polarization is maintained and when it is scrambled.

Uesugi *et al.* (30), Cotter (31) and Aoki *et al.* (32) have all measured the dependence of the transmitted and reflected powers upon the pump power and reported similar results. Figure 6 shows Aoki *et al.*'s results. They found that the transmitted power went up linearly with coupled power until 20 mW entered the fiber, at which time it became nonlinear. When the input power exceeded 30 mW, the transmitted power remained constant at 1 mW. The backward propagating power

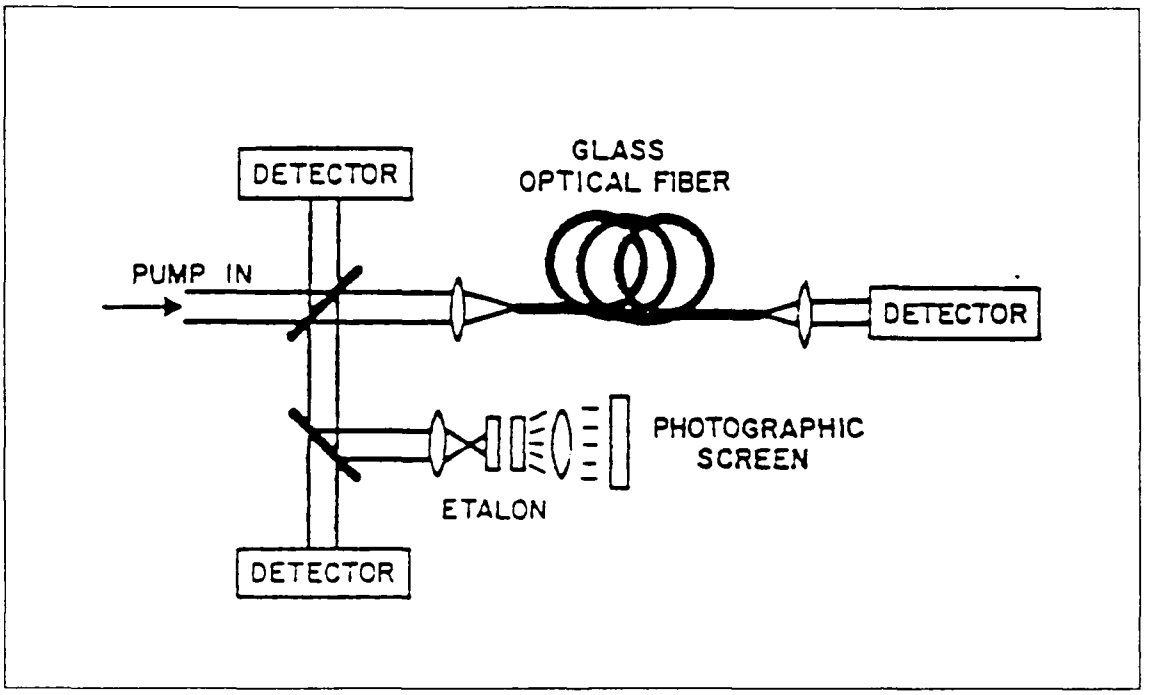

Figure 5. Typical experimental setup for the observation of SBS in single-mode fiber. From Ippen and Stolen, reference (25).

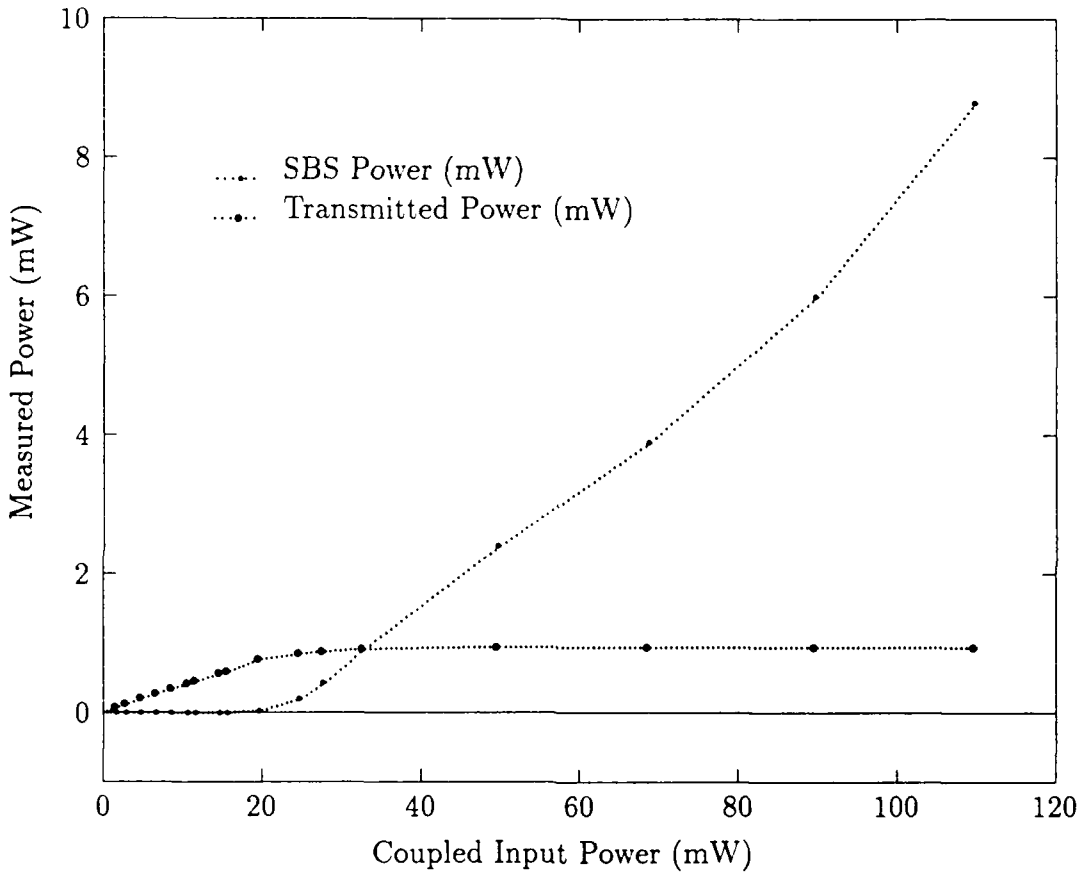

Figure 6. Power emitted from the input and far ends of a 30 km single-mode fiber as a function of launched power at a pump wavelength of 1.3 μm. From Aoki *et al.*, reference (32)

increased linearly at low input power due to Fresnel reflection from the fiber end face. However, as coupled powers exceeded 9 mW, the backward propagating power increased nonlinearly. (The scale of Figure ?? obscures this.) It became linear again at about 20 mW with a rate of increase determined by the Fresnel reflection and SBS conversion efficiency. These changes in linearity indicate that the SBS threshold was at 9 mW.

Fluctuations in the SBS and transmitted powers have been widely reported. When Ippen and Stolen first reported SBS in fiber, they noted a fluctuation in SBS power whose period depended upon the fiber length (25). The oscillations were determined to have a period equal to the round trip time of light in the fiber or its harmonics by Bar-Joseph *et al.* (16). Harrison *et al.* observed fluctuations and found that they had bursts of chaos (33).

Parameters from some of the previous SBS experiments are given in Table 1. For the experiments listed, the right side of Eq 29, which was approximated as 21, ranges from 16.6 to 21.0. The peak gain, accounting for the factor of two due to polarization scrambling, ranges from 1.4 to 8.1. Conversion efficiencies up to 80% were achieved by Aoki *et al.* (32).

Thomas *et al.* found that the gain bandwidth in a 3 μm core diameter fiber at 514.5 nm was 140 $\pm$ 20 MHz (6, 5). This is in agreement with the value of 145 MHz that Pelous and Vacher found in bulk silica (38). However, Shibata *et al.* (39) and Azuma *et al.* (40) found that the bandwidth was larger by a factor of two to three for different wavelengths and fiber core diameters. They claimed this was due to inhomogeneities in the fiber as well as to finite geometry effects. The Stokes bandwidth was found by Boyd (28) and Thomas *et al.* (6) to narrow as the SBS wave grew due to gain narrowing in a similar effect to that which occurs in lasing. Finally, Shibata *et al.* showed that the fiber's refractive index profile and core dopant level can have a strong influence on the spectral shape and center frequency of the Brillouin gain (41).

Table 1. Published Experimental Threshold Conditions for Stimulated Brillouin Scattering in Fiber

Reference	Author	Wavelength (μm)	Losses (dB/km)	Length (m)	αL	L_{eff} (m)	Core Diameter (μm)	Measured Threshold (mW)	Measured g_B ($\times 10^{-9}$ cm/W)
(25)	Ippen*	0.5355	1300	20	6.0	3.3	4.15	1000	8.14
(25)	Ippen*	0.5355	1300	5.8	1.7	2.7	4.15	2300	4.49
(31)	Cotter	.32	0.41	13600	1.3	7635	7.7	5	4.04
(31)	Cotter	1.32	0.55	31600	4	7732	7.7	6	3.34
(34)	Bolle	1.3 (?)	0.38	10000	0.87	6679	11.6	18.9	4.85
(35)	Aoki	1.32	0.46	30000	3.18	9042	11.5	9	4.36
(36)	Aoki	1.32	0.46 (?)	10000	1.06	6166	9.0	13.5	2.71
(32)	Aoki	1.32	1.1	35000	8.9	3952	11	50	1.8
(4)	Labudde[1]	0.5145	20	53	0.2	47	3.3	84	2.8
(4)	Labudde[2]	0.5145	20	53	0.2	47	3.3	60	2.5
(30)	Uesugi	0.710	4	3800	35	1054	3.5	22	1.4
(29)	Stolen	0.5145	43	395	3.9	99	2.6	68	2.7

* Pulsed excitation. [1] 30% feedback at the input. [2] 10% feedback at the input.

SBS has not been reported in multimode optical fiber as yet. It follows that phase conjugation in fiber has not been reported either, since single-mode fiber can only support one spatial mode.

V. Experimental Results and Discussion

This chapter includes a description of the experimental procedures used, the results obtained and discussion. The chapter is separated into portions concerning the experimental setup, the losses in the fiber, the transmitted and SBS power, the SBS threshold's dependence upon fiber length and feedback conditions, the fluctuations in the SBS power, the SBS frequency shift and bandwidth, spatial phase conjugation and the SBS polarization state.

5.1 Experimental Setup

In the present experiment, a single-mode argon-ion laser (Spectra-Physics Model 171) at 514.5 nm was coupled into 8.3 μm core diameter, step-index optical fiber (Corning Corguide SMF-28(TM)). The experimental set-up is shown in Figure 7. It is practically identical to the setup used to investigate SBS in single-mode fiber (without phase conjugation) (25, 1).

The laser (with etalon) had a maximum power of about 3 W and was vertically polarized. The beam diameter was 1.5 mm with a full-angle divergence of 0.5 mrad. A Faraday isolator (Optics For Research IO-5-VIR) was used to prevent the SBS beam and the reflection from the fiber input face from affecting the operation of the laser at the cost of 20% less available power. Both beamsplitters were used at near-normal incidence to minimize the effect of polarization on their transmission characteristics. The resulting difference was less than one percent. BS1 and BS2 had transmittances of 92% and 59%, respectively. A 10X microscope objective coupled the pump beam into the fiber. The fiber's numerical aperture was 0.12, so it supported nine spatial modes, in accordance with Eqs 5–8.

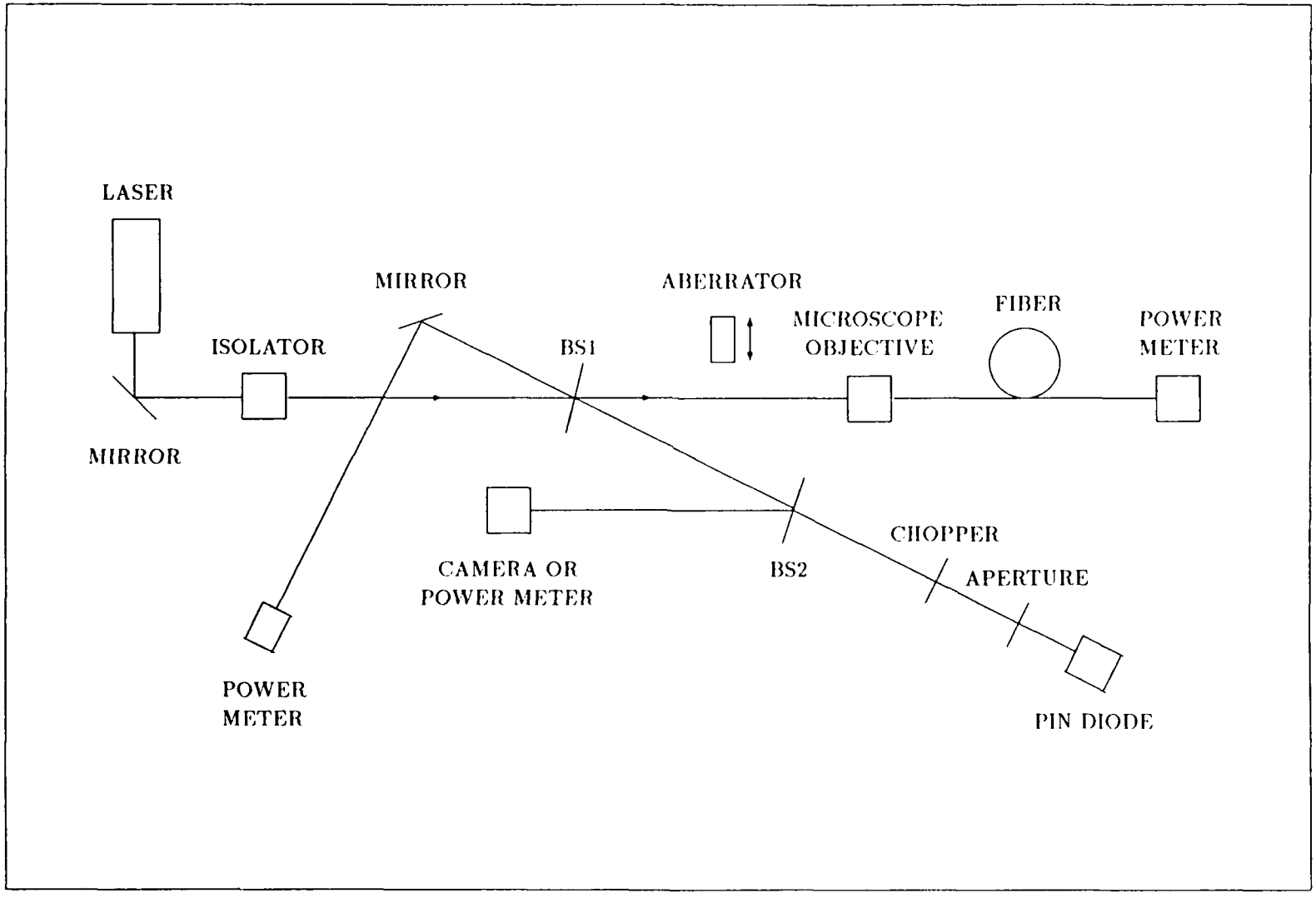

Figure 7. Schematic diagram of the experimental setup for the investigation of optical phase conjugation via SBS in multimode fiber.

5.2 Fiber Losses

The first experimentally determined fiber parameter was the power attenuation as light propagated down the fiber. The loss coefficient α was calculated from the transmission of fibers ranging in length from 97 to 720 m long using

$$P(L) = C_o P(0) \exp(-\alpha L) \tag{35}$$

where $P(0)$ is the power incident on the microscope objective, $P(L)$ is the power transmitted at the output end of the fiber and C_o is the coupling efficiency. Both C_o and α are initially unknown. However, a good estimate of C_o was obtained by repeatedly measuring the transmission of a 2 m fiber. For the objective lens used in this experiment, coupling efficiencies were consistently 0.66–0.72. These loss measurements were done using incident powers below the SBS-threshold power. A Fabry-Perot interferometer connected to an oscilloscope was used to verify that the backward travelling Fresnel reflection did not contain any frequency-shifted component.

Figure 8 shows the calculated loss coefficients α for each fiber length both when C_o is assumed to be 0.66 and when C_o is assumed to be 0.72. The two curves diverge at the higher trial numbers because the data is arranged in order of decreasing fiber length and an error in the assumed value of C_o affects the calculated value of α greater for shorter fiber lengths. The only loss coefficient which fits the expected coupling range for all the data points is 3.78×10^{-5} cm^{-1} (16.4 dB/km), which is also shown. The estimated error is 2%.

However, when the transmittance was measured at multimode powers above about 2 W, the losses varied with the light intensity and over time. Again, a Fabry-Perot interferometer connected to an oscilloscope showed no evidence of SBS during the measurements. Even several days after these measurements were made, the losses in the fiber at low power were about 24 dB/km.

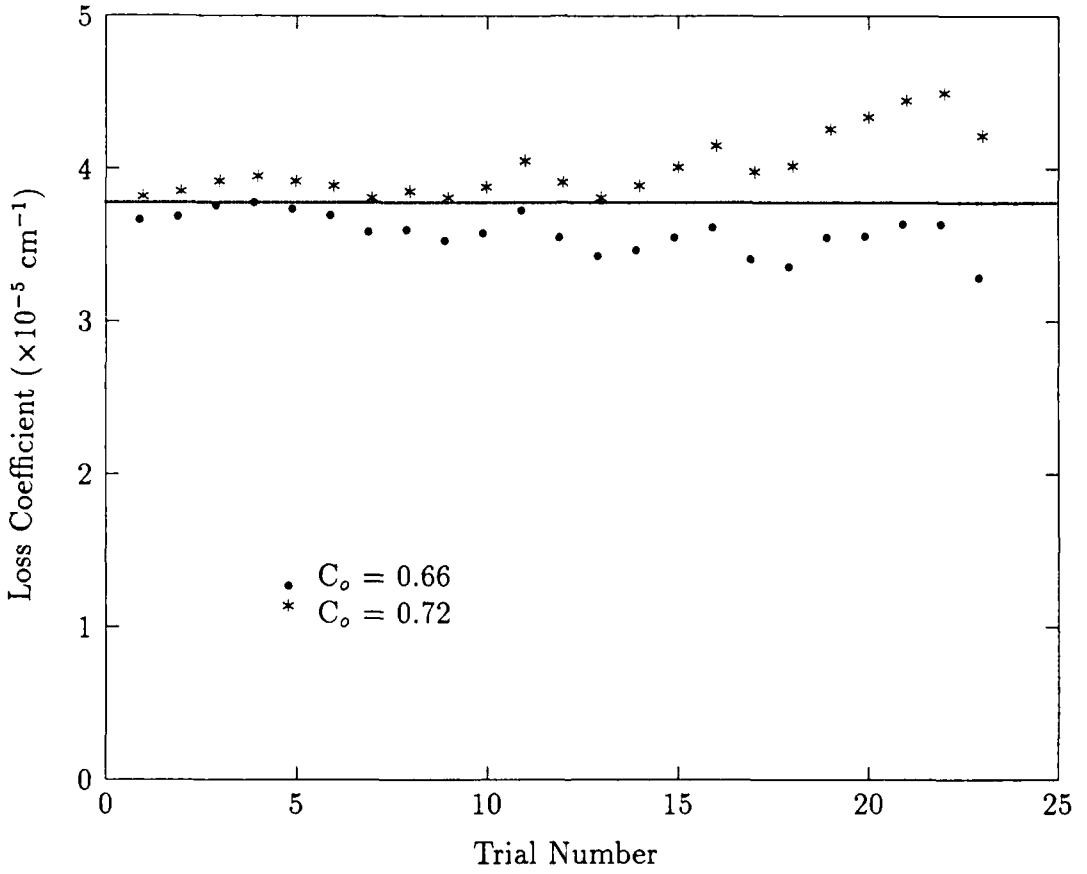

Figure 8. Fiber loss coefficient measured in fibers of varying lengths assuming coupling efficiencies of 0.66 and 0.72, the expected range. The horizontal line corresponds to losses of 3.78×10^{-5} cm^{-1} (16.4 dB/km).

The fiber losses measured here at a wavelength of 514.5 nm are slightly less than previously reported values which are in the 20–50 dB/km range. The increased losses at higher power levels in the present experiment have been reported by Stolen *et al.* (42) and investigated by Sigel (43). This phenomenon is not believed to have affected any of the results of this thesis because no fiber which had been exposed to high intensity light was used for subsequent quantitative experiments.

5.3 Transmitted and SBS Power Evolution

The evolution of the transmitted and SBS powers as the pump power was scaled was investigated next using fibers 97 m and 200 m long. Neither an index-matching liquid nor an aberrator was used.

Figure 9 shows the results for the 200 m fiber with the background light levels having been taken into account. The transmitted power increased linearly until about 280 mW entered the fiber. Thereafter, for every run it declined slightly then rose slightly, although the difference between runs is larger than the changes in power. At low input power the backward propagating power increased linearly. As coupled powers exceeded 260 mW, the backward propagating power briefly increased nonlinearly. At higher coupled power, the backward power again increased linearly, although with a larger slope than previously, except for a dip at the highest coupled powers. This indicates that the SBS threshold is about 260 mW. Appendix B contains tables of data from this section and plots for the 97 m trial, which exhibited similar results.

This behavior is similar to that previously reported for single-mode fiber (see Figure 6) (30, 31, 32). Above SBS threshold, the increasing Stokes wave drains power from the pump wave at a rate slightly faster than the increase in coupled power because the conversion efficiency is partially determined by the product of the pump and SBS intensities. Thus the transmitted pump power declines slightly. The slight rise in transmitted power at the highest coupled powers is due to the reflection

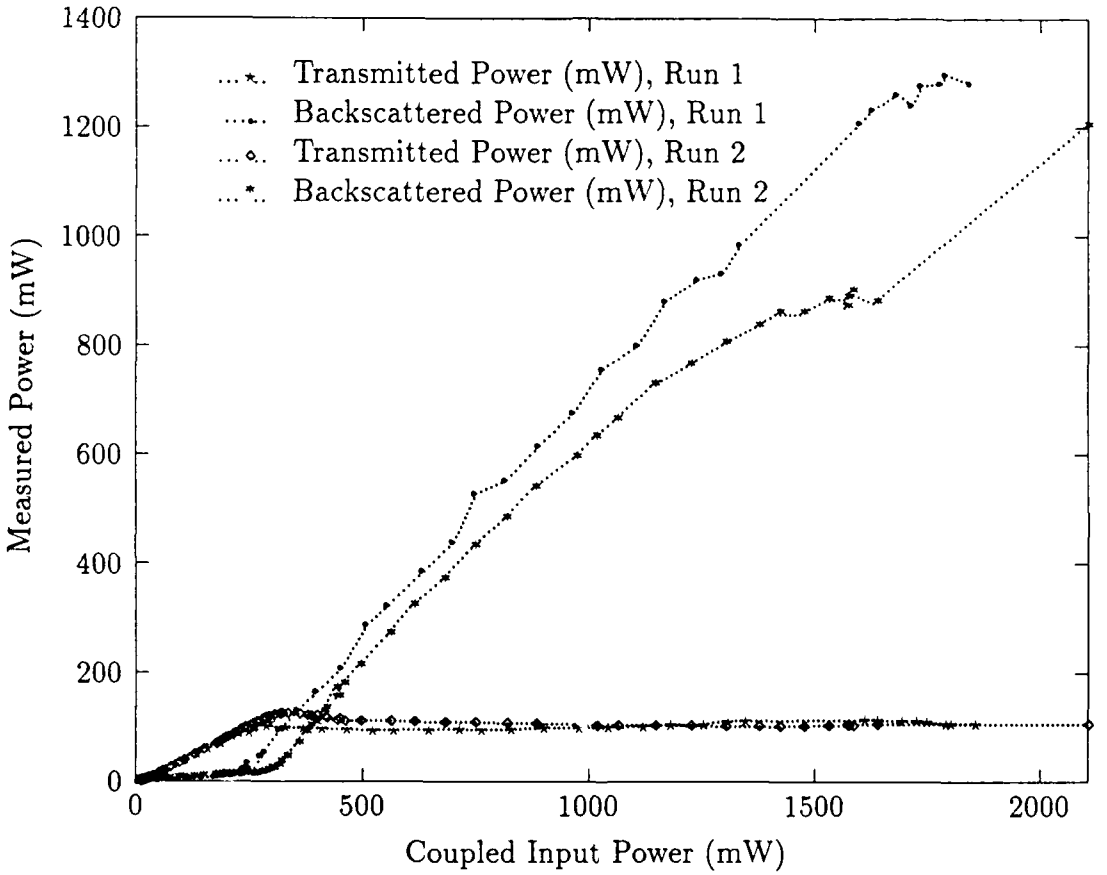

Figure 9. The evolution of the transmitted and backscattered powers as the pump power is scaled in a 200 m fiber. The results from two runs are displayed.

of the Stokes wave off the input fiber face and back out the far fiber end. This was verified by a Fabry-Perot interferometer connected to an oscilloscope detecting a second peak in the transmitted power which was shifted by about 33 GHz. The increase in the transmitted power at the highest coupled powers could also be due to the Stokes wave itself acting as a pump to a second Stokes wave. A second Stokes wave was not detectable on the oscilloscope because the width of the first Stokes peak swamped any signal which might have been shifted by an additional 33 GHz. Extrapolating Labudde *et al.*'s results for singlemode fiber, a second SBS peak should be generated approximately when the Stokes power equals twice the threshold power for the first Stokes generation (4). This is at about 1.8 W of coupled power, where the slight rise in transmitted power occurred.

At low input power the backward propagating power increases linearly due to Fresnel reflection from the fiber end face. At higher coupled power, the backward power increases linearly at a rate determined by the sum of the Fresnel reflection and the SBS conversion efficiency. The conversion efficiency is calculated by subtracting the Fresnel reflected power from the backscattered power, then dividing by the coupled input power. The Fresnel reflectivity can be determined by requiring that the SBS conversion efficiency below threshold to average zero. The calculated reflectivities were 0.044 and 0.037 for runs 1 and 2, respectively, with the difference resulting from slightly different coupling orientations into the fiber. The maximum possible reflectivity is about 0.08: 0.04 each from the microscope objective and the fiber.

Figure 10 shows the SBS conversion efficiency for both 200 m runs. It initially increased nonlinearly then leveled off at about 70% and 60% for runs 1 and 2, respectively, followed by a dip. The decrease in conversion efficiency at the end of each run could be due to a decrease in coupling efficiency, to the fiber sagging as it heats up, or to increased fiber losses. Another possibility is that a second Stokes wave was draining the power from the first Stokes wave. The estimated error in the

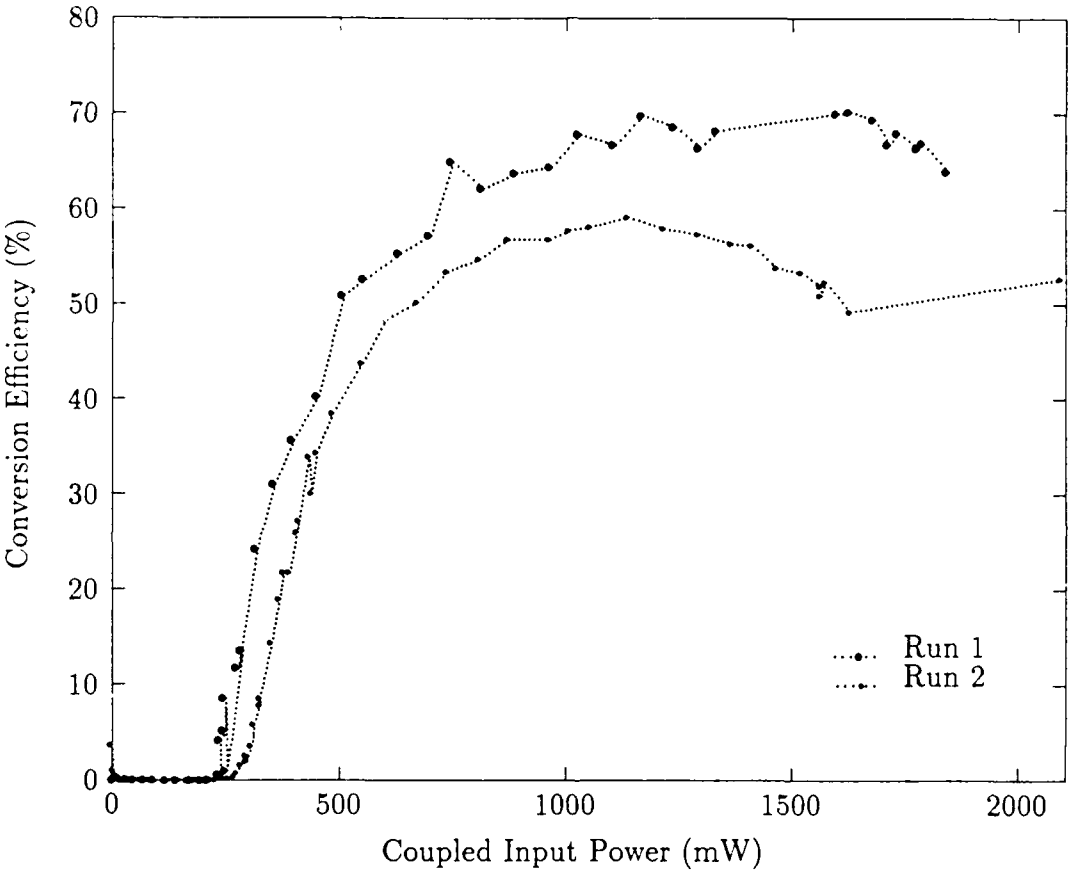

Figure 10. Conversion efficiency of the SBS process in a 200 m fiber. Two runs are shown.

data is: coupled pump power, ±5%; transmitted power, ±5%; backscattered power, ±20%; and SBS conversion efficiency, ±20%.

5.4 SBS Threshold Dependence upon Fiber Length and Feedback Conditions

The threshold power for the onset of SBS was investigated as a function of the fiber length. The onset of SBS was indicated by detection on an oscilloscope (Lavoie Laboratories Model LA 265A) of a Stokes peak coming from a Fabry-Perot interferometer (Tropel Model 240). This level of detection corresponded to 0.05 mW of SBS power leaving the fiber and passing the microscope objective. For each fiber length the threshold was found both without index-matching (4% reflection at the fiber-air interface) and with partial index-matching by immersing the far end of the fiber in water (0.4% reflection). The threshold values are calculated by multiplying the power incident on the microscope objective when SBS was detected by the coupling efficiency, which is calculated using Eq 35 assuming a loss coefficient of 16.4 dB/km.

Figure 11 shows that: (1) the threshold increases as the fiber length decreases and (2) the threshold without index-matching is less than or equal to the threshold with partial index-matching. Note that these thresholds are lower than those found in the power evolution experiment (Section 5.3) due to the different way in which the threshold is defined. The superposition of a small power increase on a relatively large Fresnel signal is harder to detect than a Stokes peak which is spatially separated from the Fresnel reflection peak on the oscilloscope.

The dependence upon fiber length, which agrees with Eq 29, is explained by the grating in the refractive index thickening when the interaction length grows. The thicker grating reflects more light. The dependence upon feedback conditions results from the modulation in the refractive index not being as deep when index matching liquid is used because less energy is kept in the fiber. The resulting weak grating reflects less light than a strong grating, which agrees with Eq 30.

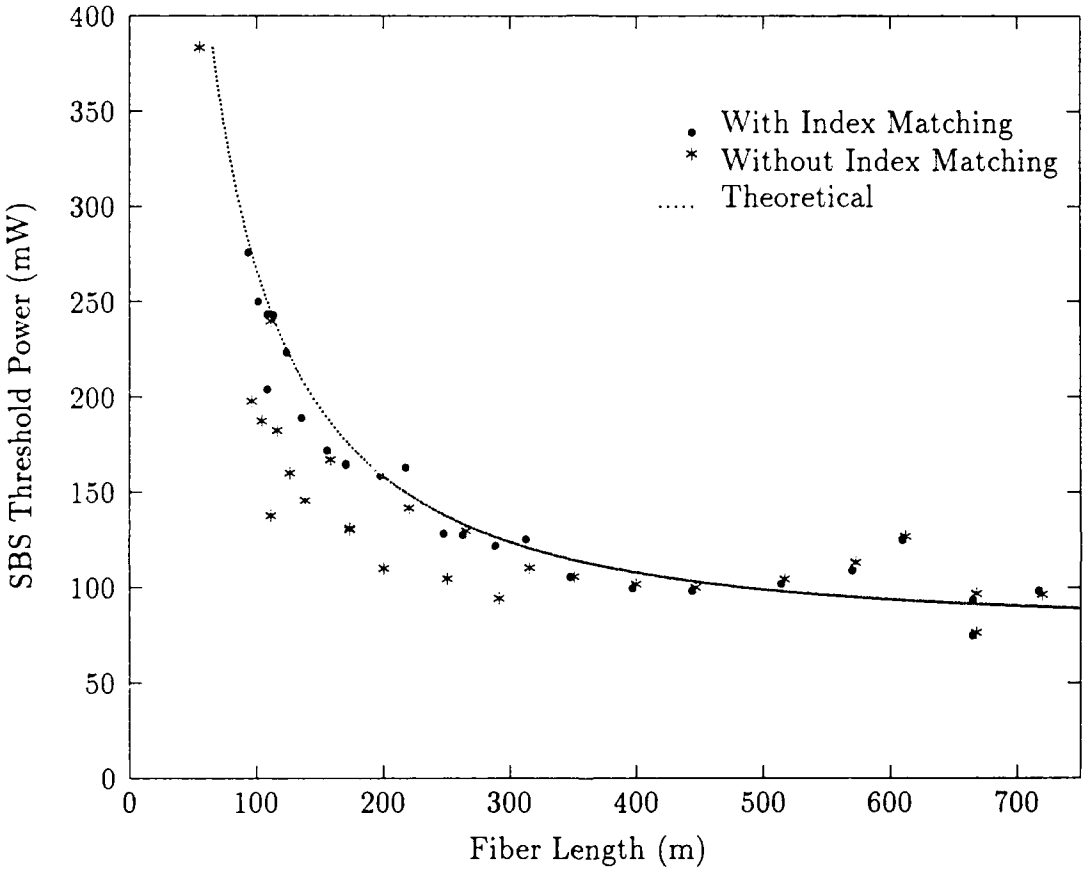

Figure 11. SBS thresholds for different fiber lengths and feedback conditions. The theoretical plot is calculated for losses of 16.4 dB/km and a gain coefficient of 10.2×10^{-9} cm/W.

The theoretical thresholds plotted in the figure, which are calculated using Eq 29 for a gain of 10.2×10^{-9} cm/W and losses of 16.4 dB/km, are close to the index-matched thresholds. This gain is larger by a factor of two than the theoretically predicted value using bulk silica parameters. The difference may be explained by the combination of finite geometry effects, different criteria for declaring threshold has occurred and the feedback present when using water to index match the fiber instead of a liquid which truly has the same refractive index (29). Since there is still a 0.4% reflection when using water, the theoretical thresholds for a given gain, which assume no feedback, are marginally higher than the measured thresholds. This raises the gain calculated from the experimental data.

The measured thresholds individually have errors of about 40% resulting from differences in coupling efficiencies and in alignment of the Fabry-Perot interferometer. A 10% change in the gain still allows the theoretical curve to fit the experimental thresholds reasonably well.

5.5 SBS Power Fluctuations

The fluctuations in the power of the SBS signal were also investigated. A PIN diode (FND-100) connected to a digital oscilloscope (LeCroy Model 9450) was used to trace the SBS intensity generated in a 200 m fiber as a function of time. The detector's response time was less than one nanosecond and the minimum period between data points is 2.5 nsec. No index-matching solution was used. The Fresnel reflection was slightly displaced from the SBS beam which enabled the SBS to be isolated using an aperture. The degree of isolation was measured by cutting the fiber at a length of two meters (after the experiment was completed) to ensure that no SBS was generated and measuring the Fresnel reflected power entering the FND-100. At maximum laser power only 3 μW of non-SBS power entered the detector compared to SBS powers ranging from 0.5–30.0 mW. At lower powers the non-SBS power entering the FND-100 decreased correspondingly. An optical chopper with a

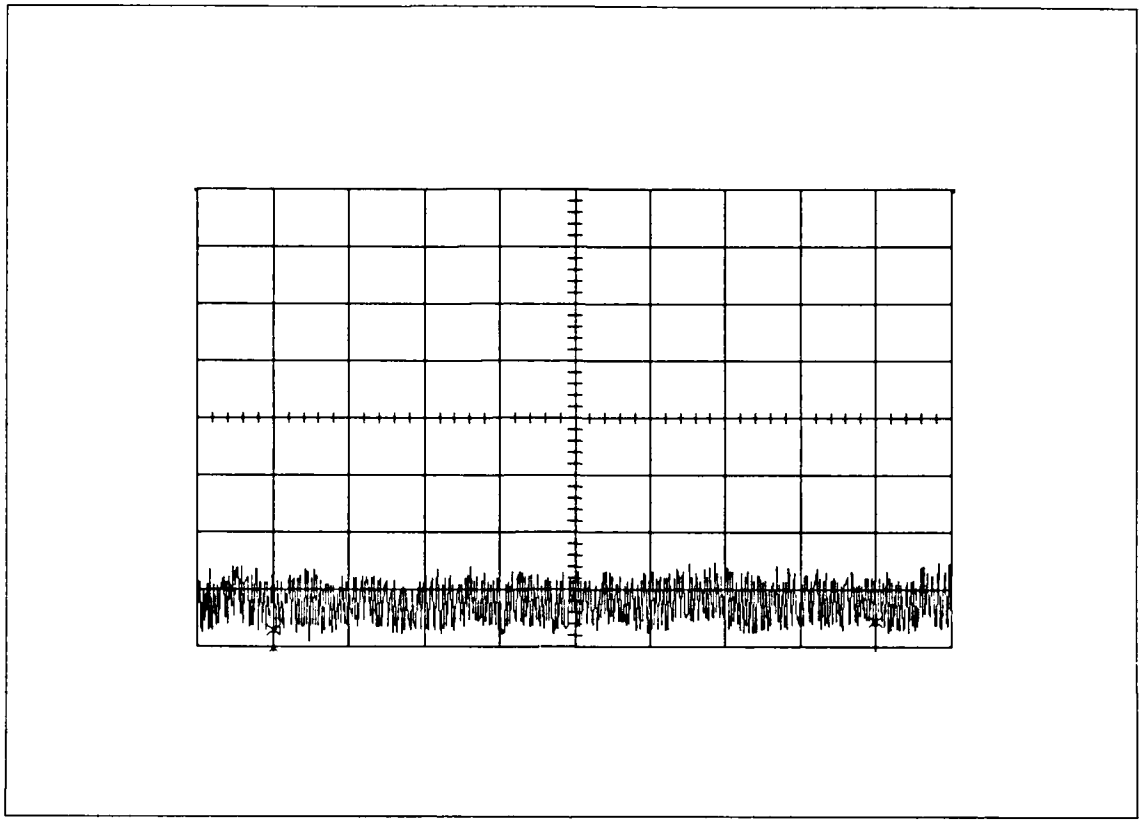

Figure 12. Laser power stability. The zero level is at the top of the graph. The horizontal scale is 0.2 sec/division.

6 msec period was placed in front of the PIN diode for some of the tracings so that the zero level could be easily distinguished.

As seen in Figures 12–15, which are all inverted, although the pump beam had only small power fluctuations (10% or less), the SBS power fluctuations varied between 10% and 100%. Relatively stable output (10% or less) occurred over intervals of about 2–8 msec. The fluctuations appear to be periodic, with two main periods in each tracing. The slower of the two fluctuations' period was either 1.91 μsec when the pump power was 1.25 times the threshold power or 0.95 μsec at higher pump powers. These periods were reproducible at a given pump power. The faster fluctuations had periods ranging of 50–210 nsec. The round trip time for light in this fiber is calculated to be about 1.93 μsec where a typical refractive index of silica

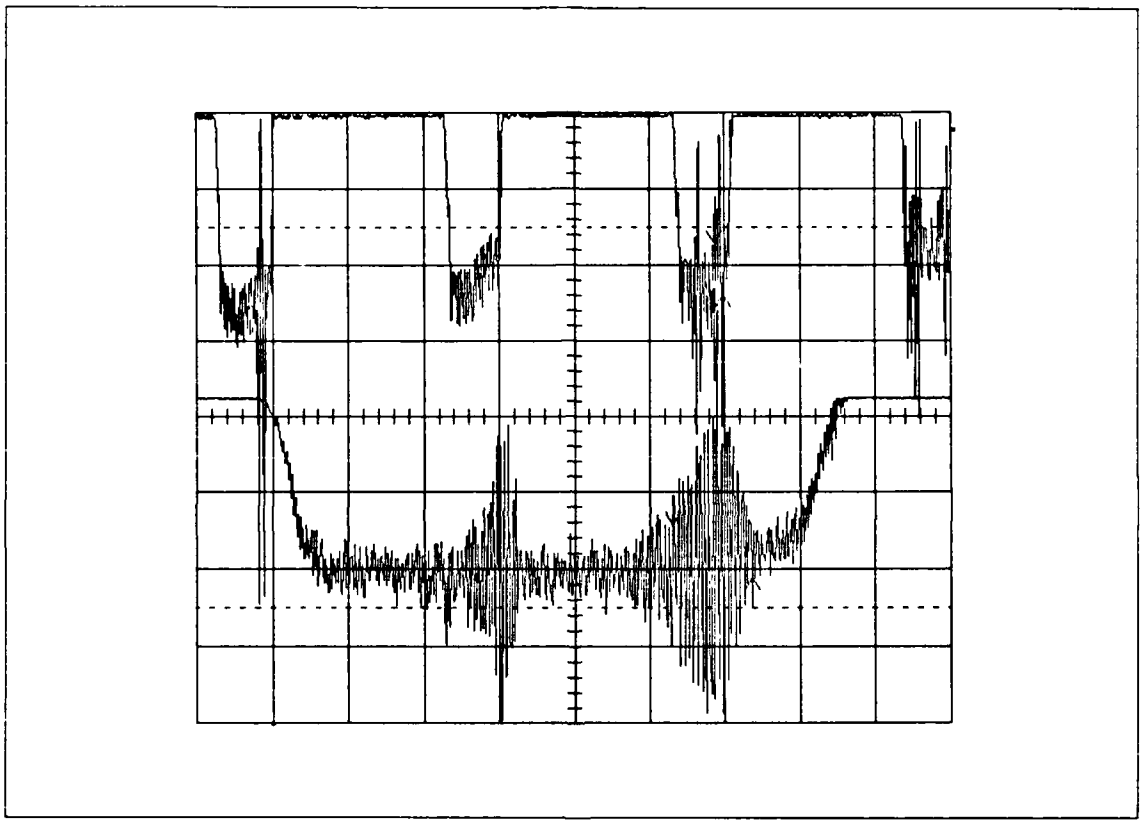

Figure 13. SBS power in a 200 m fiber as a function of time. A chopper has been used to easily identify the zero level. A power meter indicated 250 mW of SBS power was in the fiber. The bottom trace (0.2 msec/division) is an expanded portion of the top trace (2 msec/division).

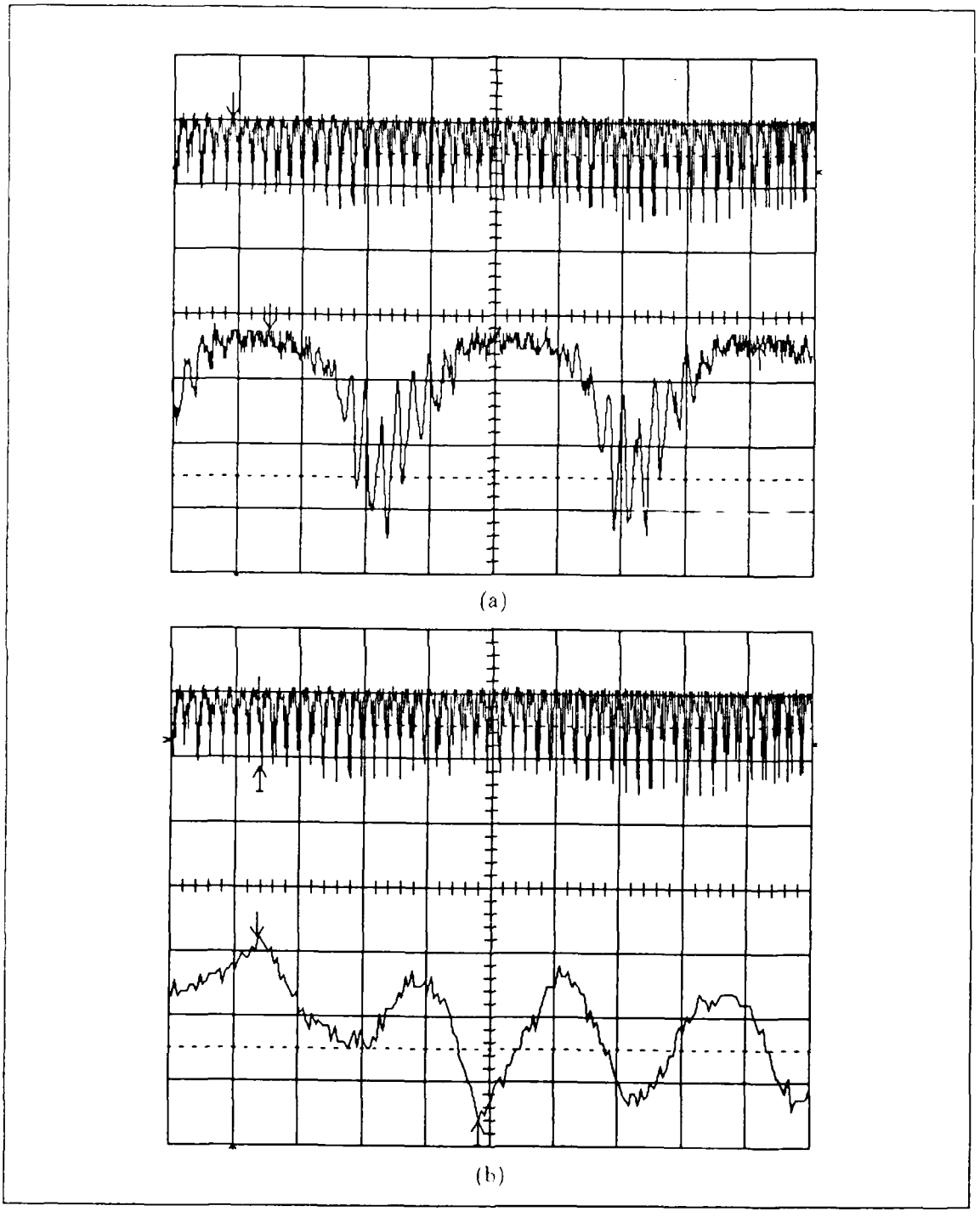

Figure 14. SBS power generated in a 200 m fiber as a function of time. A power meter indicated 17 mW of SBS power was in the fiber. The top trace (10 μsec/division) has been expanded to (a) 0.5 μsec/division and (b) 0.05 μsec/division.

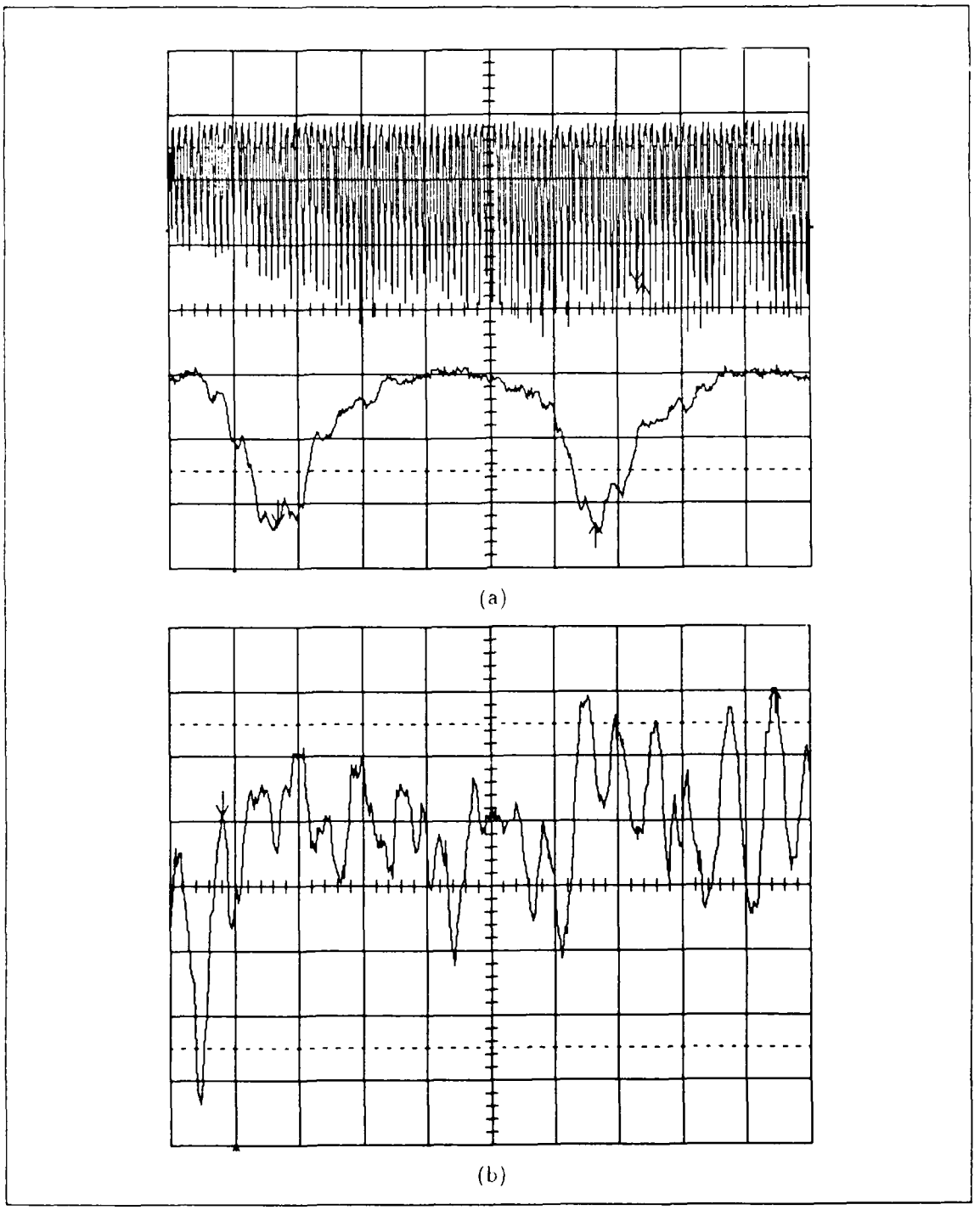

Figure 15. SBS power in a 200 m fiber as a function of time. A power meter indicated 19 mW of SBS power was in the fiber. The top trace (10 μsec/division) has been expanded to (a) 0.2 μsec/division and (b) 0.1 μsec/division.

fiber (1.46) has been used.

SBS power fluctuations with periods equal to the round trip time in the fiber or its first harmonic have been widely reported and are due to changing depletion rates in the pump wave at different positions along the fiber (25, 16). The fluctuations with periods ranging from 50 nsec to 210 nsec have only recently been reported along with bursts of large fluctuations by Harrison *et al.* (33). Phase portraits and power spectra were not generated for our data, so it is not known if the bursts were chaotic. There is no clear tie to the slower fluctuations.

5.6 SBS Frequency Shift and Bandwidth

The frequency shift was determined using the combination of a wavemeter (Burleigh Model WA-10) and a Fabry-Perot interferometer feeding a digital oscilloscope. The wavemeter gave the shift with an uncertainty of 0.6 GHz. However, the oscilloscope gave accuracies within 0.02 GHz, but only assuming the frequency was known to within 1.5 GHz, the free spectral range of the Fabry-Perot interferometer. The shift on the oscilloscope, which was calibrated using the separation between successive laser (and SBS) peaks of 1.5 GHz, gave a shift of $1.28 \pm 0.02 + (1.5)m$ GHz where m is a nonnegative integer. The wavemeter measured a Stokes shift between 32.4 and 33.6 GHz. Thus the SBS shift was 32.78 GHz with an error of 0.02 GHz. This value is slightly less than both the theoretical value of 33.8 GHz for bulk silica and the value of 33.90 ± 0.05 GHz measured by Thomas *et al.* in a 3 μm core diameter fiber (6). The difference in guided acoustic wave speeds probably accounted for the difference (6, 41).

The bandwidth of the laser and SBS was measured using the same oscilloscope trace. They were found to be 12 MHz and 16 MHz (at 4.5 times SBS threshold), respectively. At 1.25 times threshold, the lowest at which the bandwidth could be measured, the SBS bandwidth was 35 MHz. The error in these bandwidth measurements is about 1 MHz.

The narrowing of the SBS bandwidth as the SBS power grows is caused by the approximately exponential gain along the fiber: the most intense frequency is amplified more than less intense frequencies which make it progressively more dominant (6, 28). The SBS bandwidth, at threshold, is the convolution of the laser bandwidth and the gain bandwidth, so the gain bandwidth is greater than 23 MHz. This lower limit is an order of magnitude smaller than previously reported bandwidths, so this result is of limited value. The laser bandwidth being smaller than the gain bandwidth means that the SBS gain was not seriously degraded from its peak value (44, 45).

5.7 Spatial Phase Conjugation

The spatial phase-conjugating ability of SBS in multimode fiber was investigated using a frame grabber system (Big Sky Beamcode with a CID camera (General Electric Model TN2509A7B)). The phase aberrator, a microscope slide etched in acid, was placed immediately in front of the microscope objective in order to distort the pump beam being coupled into the 3.6 km fiber. The distorted Fresnel reflection and distorted SBS beam subsequently re-traversed the aberrator in the opposite direction. For a perfectly phase-conjugate SBS beam, the aberrations introduced by the phase plate should have been exactly compensated and the image recorded at the camera should have matched the initial unaberrated diffraction-limited pump image. However, as the phase-conjugate fidelity of the SBS beam decreased, the image should have appeared progressively more distorted. The Fresnel reflection was distorted twice by the aberrator. Figure 16 shows power contour lines for (a) the pump beam, (b) the reflection of the pump beam from the input end of the fiber without the aberrator and below SBS threshold, (c) the reflection of the pump beam from the input end of the fiber with the abberator and below SBS threshold and (d) the SBS beam with the abberator in front of the microscope objective and a neutral density filter (ND 1) in front of the camera. A comparison of the reflected beams

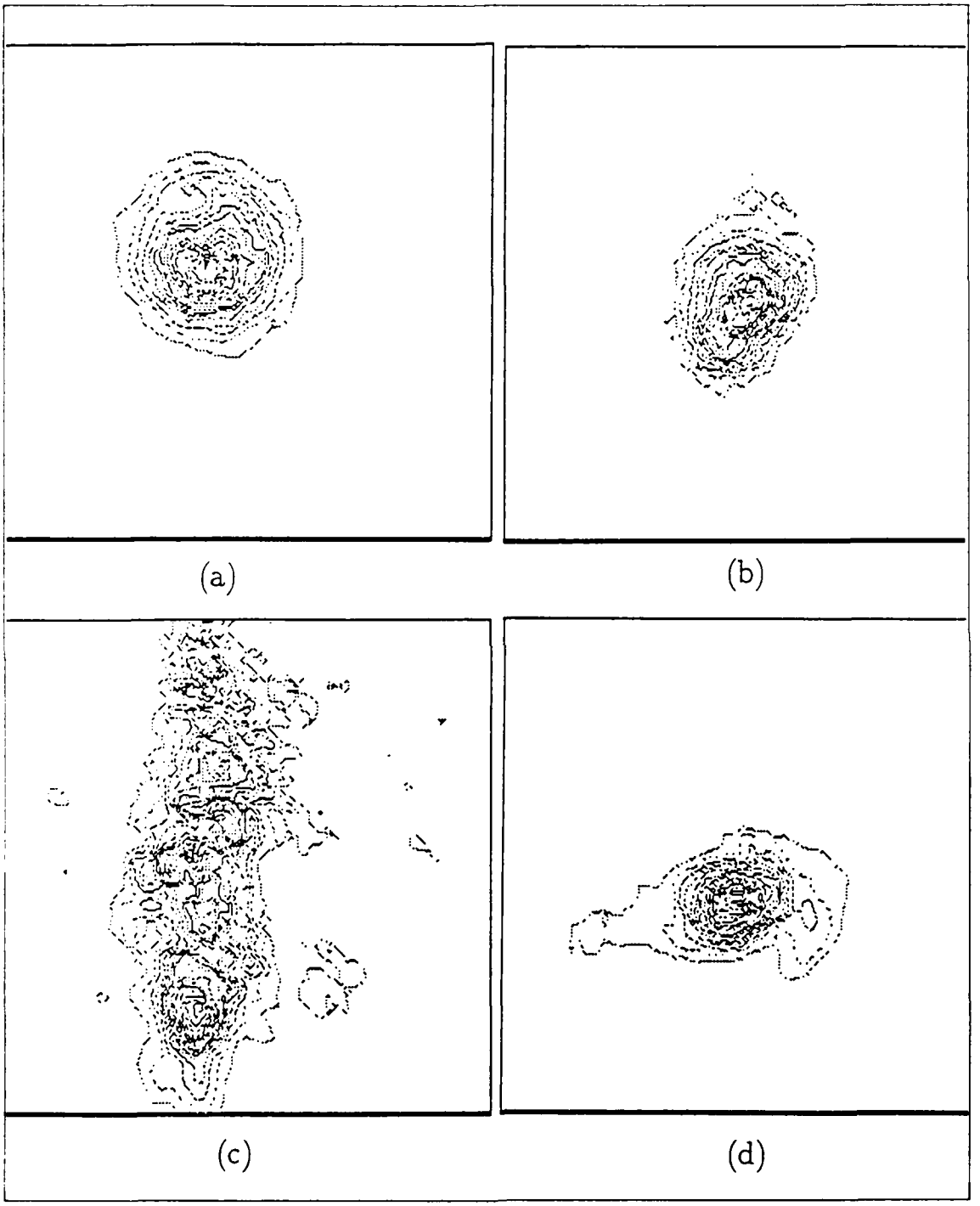

Figure 16. Frame grabber recordings of beam intensity contour profiles: (a) input laser beam; (b) the Fresnel reflection from the input face of the fiber; (c) aberrated Fresnel reflection from the input fiber face; (d) aberration-corrected SBS beam.

with and without the phase plate shows that the aberration arose mainly due to the phase plate. The slight distortion in the unaberrated Fresnel reflection from the fiber is due to an imperfect fiber cleave.

Each picture was taken at near maximum camera response in order to maximize the number of contour lines. This was done by scaling the pump power in Figures 16(a)-16(c). Figure 16(d) was taken at maximum laser power, which was two to three times SBS threshold. Although Figures 16(b)-16(d) were taken at the same point, the camera was moved before taking Figure 16(a). Even if the camera distances from beam splitter were the same, the SBS and pump diameters cannot be compared directly—the SBS conjugate beam is converging toward the camera while the pump beam is diverging and the neutral density filter widens the SBS beam. After corrections are made for these effects, the diameters at $\exp(-2)$ of the peak power were 1.3 mm $\times$ 1.4 mm for the pump beam and 2.0 mm $\times$ 1.3 mm for the SBS beam. The aberrated reflection was approximately 2.1 mm $\times$ 8.8 mm. In addition to the nearly phase-conjugate peak, weak portions of the SBS beam were spread over the camera frame. Thus, although the aberration correction was not perfect, it did occur.

The SBS beam did not change shape or position over time, even when the aberrator was moved by hand. Neither varying the angle of linear polarization of the pump beam nor putting the far fiber end in water affected the phase-conjugate fidelity. The same results were found and videotaped using a 200 m fiber, although at times the fidelity was markedly reduced.

Further investigations as to why the phase-conjugate fidelity was markedly reduced for some trials are required. Which parameters caused the nearly phase-conjugate beam to be degraded should also be investigated. The possibility that the power reflected at the far fiber end interferes with the grating formed in the refractive index seems to be eliminated by the fidelity's independence from feedback variations. Although the peak of the Fresnel reflection was only one-tenth as intense

as the SBS peak and was located outside Figure 16(d)'s frame, some of the distortion from Gaussian could also perhaps be attributed to it. Another reason the aberrations were not completely eliminated may have been that the core diameter of the fiber used was only 8.3 μm. A wider core would have allowed higher spatial frequencies into the fiber to be conjugated. It would also be possible to use a bundle of fibers to sample the wavefront over an even larger area. Some information would be lost and the threshold power would increase but the power handling capabilities would rise and much higher frequencies could be conjugated. However, there may be a problem with lack of coherence between fibers with the bundle idea.

5.8 SBS Polarization State

In some applications the pump beam's polarization must be conjugated as well as the spatial frequencies. Therefore, the polarization state of the SBS beam was briefly investigated without the phase plate in the beam. A sheet polarizer and a power meter (Newport Model 815) were used to measure the angle and degree of polarization of the SBS beam as the linear polarization of the pump was rotated using a half-wave plate. The polarization angle of the SBS was determined by rotating the polarizer until the maximum power passed to the power meter.

Some error is introduced because the reflection off of the fiber was in approximately the same location as the SBS beam. However, this experiment was done with the SBS signal being five to ten times as intense as the four percent fiber reflection, so this particular error is small. A much larger error, up to 40°, was caused by 20% fluctuations in the SBS power readings.

The SBS polarization angles for 97 m and 3.6 km fibers were found to be apparently random. No clear dependence was shown relative to a stationary frame of reference either, which shows that there is no preferred polarization angle in the fiber. In addition, the SBS power did not reproduce the linear polarization of the pump beam. Therefore, when using optical fiber, a large portion of the SBS

polarization does not reproduce the polarization state of the pump beam.

This is due to polarization scrambling occurring in the fiber. Polarization scrambling is caused by deformations of the core from circular or to anisotropy of the fiber material. These nonuniformities allow the longitudinal components of the electric fields of orthogonally polarized modes to exchange power and cause the propagation constants of the modes to differ (46:157–159).

When the polarizer was rotated, the SBS intensities changed over the whole frame at the same rate. This shows that the polarization of the phase-conjugate peak was spatially uniform.

VI. Conclusion

The main objective of this thesis was to obtain phase conjugation of an argon-ion laser beam using the process of stimulated Brillouin scattering (SBS) in multi-mode optical fiber and to characterize the parameters involved.

This was accomplished at a wavelength of 514.5 nm in an 8.3 μm core diameter fiber. The loss coefficient of the fiber was found to be 16.4 $\pm$ 0.3 dB/km for low power levels and to increase when the fiber was exposed to powers above about 2 W.

The transmitted and backscattered powers exhibited behavior similar to that previously reported for single-mode fiber with the SBS conversion efficiency reaching as high as 70% in a 200 m fiber. The expected dependences of the SBS threshold upon fiber length and feedback conditions were also seen: the threshold increased both when the fiber length decreased and when index matching liquid was used. The measured gain coefficient with 0.4% reflection at the far fiber end was found to be 10.2×10^{-9} cm/W with an estimated error of 10%. This is somewhat larger than the reported values for single-mode fibers of 1.4–8.1 $\times 10^{-9}$ cm/W at wavelengths between 0.5145 and 1.32 μm. The measured Stokes shift of 32.78 $\pm$ 0.02 GHz is slightly less than the commonly reported value of 34 GHz. Narrowing of the SBS bandwidth with increasing power was observed, as expected, and the gain bandwidth was shown to be at least 23 MHz, which easily agrees with previously reported values.

Some of the SBS was not spatially phase-conjugate to the pump wave but most of it did show the ability to correct phase aberrations in the optical path. Neither moving the aberration by hand nor putting the far end of the fiber in water affected the phase-conjugate fidelity.

However, a large percentage of the SBS power did not reproduce the linear polarization of the pump wave and if any of the SBS was linearly polarized it was probably not at the same angle as that of the pump beam. In addition, strong

fluctuations in the SBS power occurred every 2–8 msec with two dominant periods. The slower period was either equal to the round trip time in the fiber (1.93 μsec) or its second harmonic and the faster fluctuations had periods of 50–210 nsec. Both of these results have been observed previously in single-mode fiber.

Thus, spatial phase-conjugation has been achieved for the first time in a multimode optical fiber, although large fluctuations in the SBS power and polarization scrambling remain as problems. Further investigations into polarization, spatial and temporal characteristics are needed, but optical fiber does seem to offer the possibility of a fast and simple phase-conjugate mirror.

Appendix A. *Method for Coupling Light into an Optical Fiber*

This appendix presents a method to couple a laser beam into an optical fiber with specific mention of the particulars used in this thesis. Efficient coupling of a 1.5-2.0 mm beam can be achieved for fibers with numerical apertures of at least 0.12 and core diameters greater then eight micrometers by using a 10X microscope objective lens (focal length = 14 mm).

First, the fiber end is stripped of its coating either mechanically (Norland No-Nik) or chemically (Zip Strip). The fiber is then cleaved. A cut within two degrees of perpendicular is achieved 98% of the time using a Fitel S-311B fiber cleaver. Next, any dust on the fiber end is removed by gently touching it with tape. The fiber is then examined under a microscope to ensure a clean cut.

The fiber and lens are placed in a five degrees of freedom lens-fiber holder (Newport F-91TS). The beam is centered on the microscope objective lens and kept at a low enough power so that the fiber coating does not burn when the beam strikes it. The fiber is adjusted horizontally and vertically until the beam is striking the fiber end. This produces a reflection travelling approximately back along the input beam. By placing a beamsplitter in the optical path the reflection can easily be separated from the input beam. The lens-to-fiber distance is adjusted until the reflection is the smallest spot possible in the far field. This means that the end of the fiber is at the focal point of the lens. Generally the lens to fiber distance will be a few millimeters. Next the horizontal and vertical fiber positions are adjusted for maximum fiber transmission. Finally, the two angular adjustments are optimized. The mount used was made so that these angular adjustments would not require readjustment of the other three degrees of freedom.

If the fiber length and losses are such that no measurable light is transmitted, increasing fiber brightness can be used as a sign of increasing coupling efficiency.

If SBS is achieved, increasing amounts of SBS power at constant pump power also indicates increasing coupling efficiency.

Appendix B. *Transmitted and SBS Power Experimental Data*

The experimentally found transmitted powers, backscattered powers and SBS conversion efficiencies used in constructing Figures 9 and 10 are given in Tables 2–4.

The experimentally found transmitted powers, backscattered powers and SBS conversion efficiencies of a 97 m fiber are graphed in Figures 17 and 18. The amount of coupled power was limited by the laser available at the time. The conversion efficiency was calculated in the same manner and the error in the data is the same as for the 200 m data. The SBS threshold is about 250 mW.

Table 2. Experimental data showing the evolution of the transmitted and SBS powers as the coupled power is increased in a 200 m fiber without index matching. Run 1, except for the first few data points.

Input Power (mW)	Throughput Power (mW)	Backscattered Power (mW)	Conversion Efficiency (%)
201.5	84.5	11.1	-0.1
216.2	89.5	12.0	0.0
217.3	91.0	12.2	0.1
240.1	91.0	14.8	0.6
241.1	102.0	23.6	4.2
249.8	100.0	26.8	5.2
250.9	100.0	35.6	8.6
255.3	102.0	16.8	1.0
287.9	108.0	55.3	13.6
279.2	103.0	48.5	11.8
320.4	100.0	95.8	24.3
359.6	99.0	131.8	31.1
400.8	98.0	165.5	35.7
455.1	97.0	208.8	40.3
510.5	95.0	288.2	50.9
557.2	95.0	324.2	52.6
634.4	96.0	386.4	55.3
701.7	97.3	440.5	57.2
750.6	96.0	528.7	64.9
817.9	96.5	553.5	62.1
890.7	99.0	616.8	63.7
967.9	99.0	677.0	64.4
1032	100.0	757.1	67.8
1109	102.0	801.2	66.7
1170	105.0	881.4	69.8
1242	104.5	921.5	68.6
1297	111.4	933.5	66.4
1336	112.0	985.6	68.2
1601	114.0	1210	70.0
1629	114.4	1234	70.2
1684	112.0	1262	69.4
1716	112.0	1242	66.8
1738	111.0	1278	68.0
1781	107.5	1282	66.4
1792	107.4	1298	66.9
1847	107.0	1282	63.9

Table 3. Experimental data showing the evolution of the transmitted and SBS powers as the coupled power is increased in a 200 m fiber without index matching. Run 2.

Input Power (mW)	Throughput Power (mW)	Backscattered Power (mW)	Conversion Efficiency (%)
1.0	0.4	0.1	3.7
4.2	1.8	0.2	1.0
8.1	3.2	0.4	0.3
12.9	5.2	0.6	0.3
14.2	5.7	0.7	0.4
17.3	7.4	0.8	0.2
20.0	8.3	0.9	-0.1
26.5	10.4	1.2	-0.3
41.2	16.5	1.9	0.0
47.5	19.4	2.2	0.0
53.1	21.3	2.5	0.1
66.4	27.0	3.1	0.0
85.1	34.5	4.0	0.0
96.6	40.0	4.6	0.0
119.7	49.9	5.6	0.0
140.5	59.5	6.7	0.1
168.2	70.0	7.9	0.0
174.8	73.6	8.3	0.0
183.4	77.5	8.6	0.0
187.8	80.4	9.1	0.1
194.9	83.0	9.3	0.1
206.3	87.0	9.7	0.0
217.1	92.5	10.4	0.1
221.5	95.9	10.7	0.1
231.2	100.0	11.1	0.1
249.7	107.5	12.2	0.2
258.4	111.0	12.6	0.2
271.4	115.9	13.7	0.4
276.9	117.8	15.3	0.8
285.6	120.5	17.9	1.6
296.4	122.7	21.5	2.6
297.5	123.0	19.9	2.0
308.4	125.0	25.5	3.6
312.7	125.5	33.0	5.9
325.7	126.0	41.1	7.9

Table 4. Continuation of Experimental data showing the evolution of the transmitted and SBS powers as the coupled power is increased in a 200 m fiber without index matching. Run 2.

Input Power (mW)	Throughput Power (mW)	Backscattered Power (mW)	Conversion Efficiency (%)
325.7	125.3	43.1	8.6
351.8	125.0	67.2	14.4
369.2	122.0	87.6	19.0
377.9	121.0	100.0	21.8
390.9	122.0	103.7	21.8
408.3	119.0	125.3	26.0
411.6	118.2	131.3	27.2
434.4	113.5	168.2	34.0
439.8	117.0	153.0	30.1
450.7	112.0	176.2	34.4
486.5	112.0	210.3	38.5
551.7	112.0	267.6	43.8
603.8	111.0	320.5	48.4
671.2	109.5	368.6	50.2
738.5	109.5	428.7	53.4
809.1	108.0	480.8	54.7
873.2	107.5	537.0	56.8
964.5	105.8	593.1	56.8
1008	104.0	629.1	57.7
1054	104.0	661.2	58.1
1137	104.0	725.3	59.1
1216	103.5	761.4	57.9
1293	102.0	801.5	57.3
1366	102.0	833.6	56.3
1412	102.0	857.6	56.1
1466	103.0	857.6	53.8
1521	104.0	881.7	53.3
1564	104.0	885.7	51.9
1564	106.0	869.6	50.9
1575	104.0	897.7	52.3
1629	106.0	877.7	49.2
2096	106.0	1202	52.7

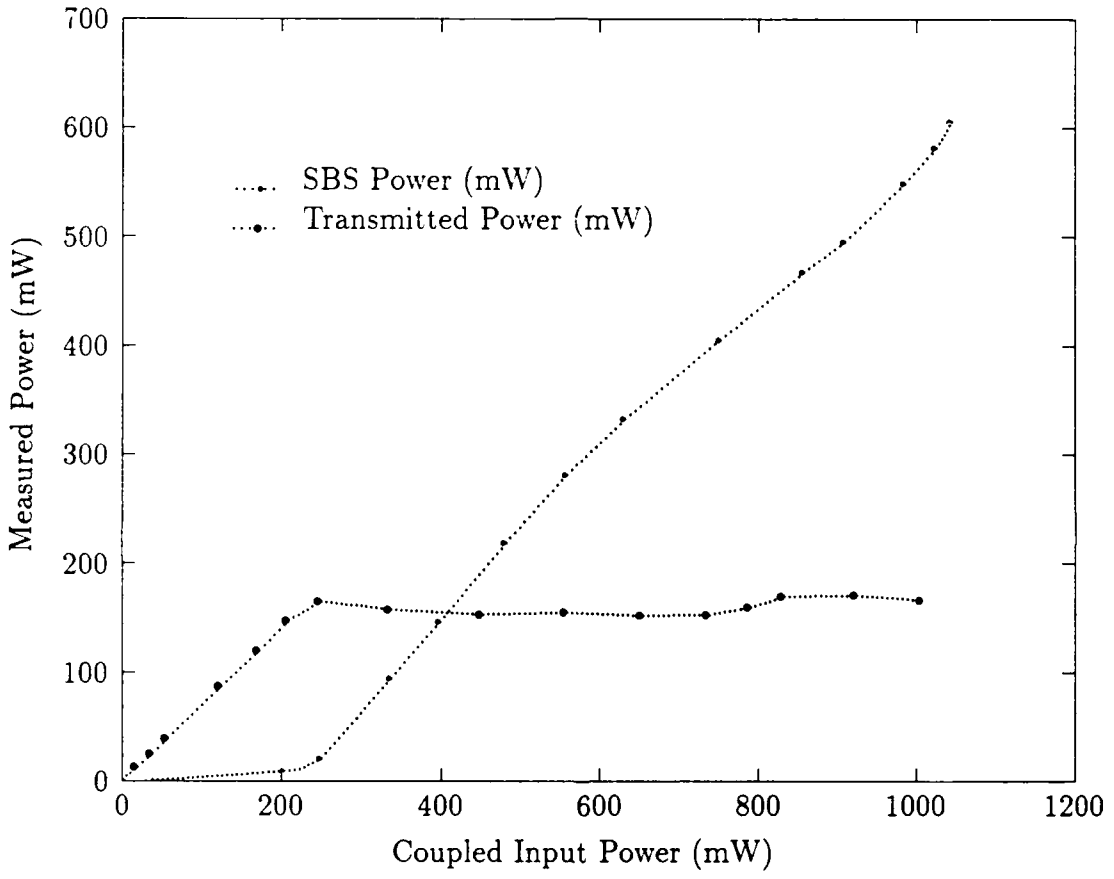

Figure 17. The evolution of the transmitted and backscattered powers as the pump power is scaled in a 97 m fiber.

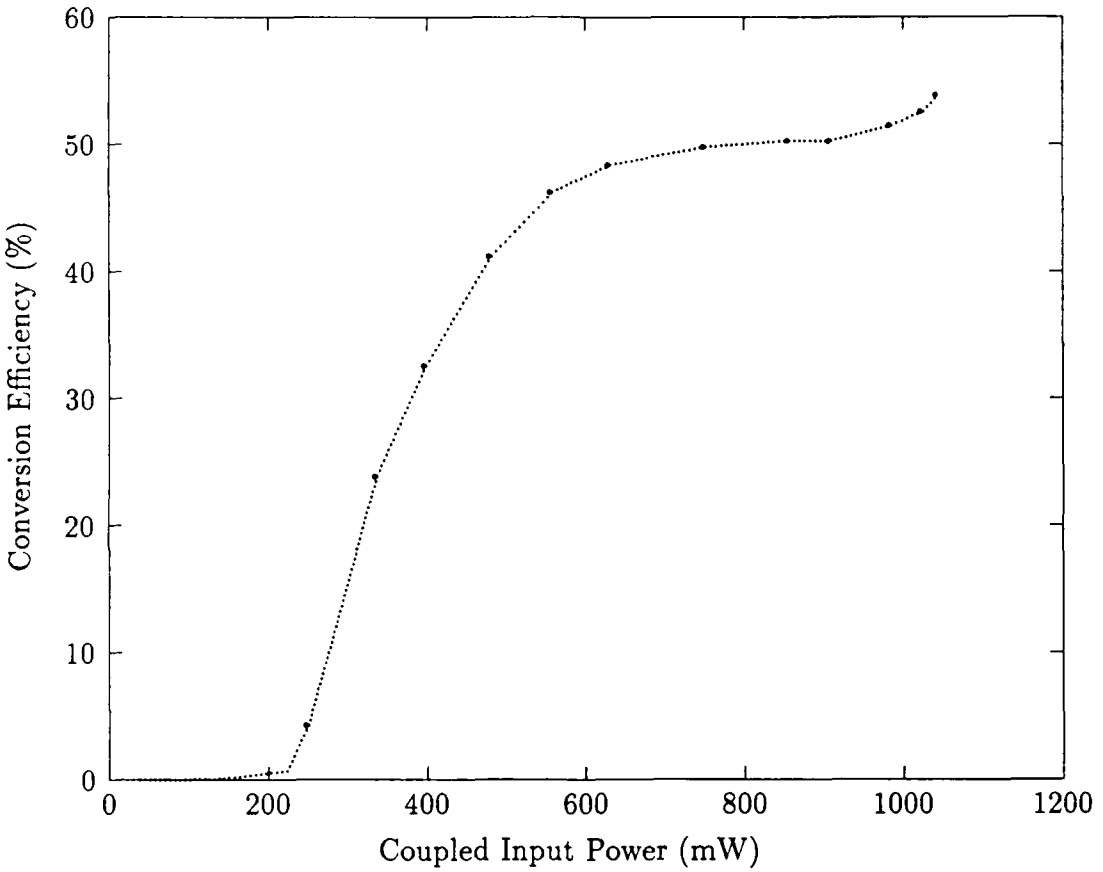

Figure 18. Conversion efficiency of the SBS process in a 97 m fiber.

Bibliography

1. D. Cotter. Stimulated Brillouin Scattering in Monomode Optical Fiber. *J. Opt. Comm.*, 4:10–19, 1983.
2. G.P. Agrawal. *Nonlinear Fiber Optics.* Academic Press, Inc., New York, 1989.
3. N.M. Kroll. Excitation of Hypersonic Vibrations by Means of Photoelastic Coupling of High-Intensity Light Waves to Elastic Waves. *J. Appl. Phys.*, 36:34–43, January 1965.
4. P. Labudde, P. Anliker, and H.P. Weber. Transmission of Narrowband High Power Laser Radiation Through Optical Fibers. *Opt. Comm.*, 32:385–390, March 1980.
5. N.L. Rowell, P.J. Thomas, H.M. van Driel, and G.I. Stegeman. Brillouin Spectrum of Single-Mode Optical Fibers. *Appl. Phys. Lett.*, pages 139–141, January 1979.
6. P.J. Thomas, N.L. Rowell, H.M. van Driel, and G.I. Stegeman. Normal Acoustic Modes and Brillouin Scattering in Single-Mode Optical Fibers. *Phys. Rev. B*, 19:4986–4998, May 1979.
7. C.L. Tang. Saturation and Spectral Characteristics of the Stokes Emission in the Stimulated Brillouin Process. *J. Appl. Phys.*, 37:2945–2955, July 1966.
8. D. Heiman, D.S. Hamilton, and R.W. Hellwarth. Brillouin Scattering Measurements on Optical Glasses. *Phys. Rev. B*, pages 6583–6592, June 1979.
9. P. Narum, M.D. Skeldon, and R. W. Boyd. Effect of Laser Mode Structure on Stimulated Brillouin Scattering. *IEEE J. Quan. Elec.*, 22:2161–2167, November 1986.
10. E. Lichtman, A.A. Friesem, R.G. Waarts, and H.H. Yaffe. Stimulated Brillouin Scattering Excited By Two Pump Waves in Single-Mode Fibers. *J. Opt. Soc. Am. B*, 4:1397–1403, September 1987.
11. E. Lichtman and A.A. Friesem. Stimulated Brillouin Scattering Excited By a Multimode Laser in Single-Mode Optical Fibers. *Opt. Comm.*, 64:544–548, December 1987.
12. G.C. Valley. A Review of Stimulated Brillouin Scattering Excited with a Broad-Band Pump Laser. *IEEE J. Quantum Electron.*, QE-22:704–712, May 1986.
13. R.G. Smith. Optical Power Handling Capacity of Low Loss Optical Fibers as Determined by Stimulated Raman and Brillouin Scattering. *Appl. Opt.*, 11:2489–2492, November 1972.

14. G.K.N. Wong and M.J. Damzen. Investigations of Optical Feedback Used to Enhance Stimulated Scattering. *IEEE J. Quan. Elec.*, 26:139–148, January 1990.

15. R.V. Johnson and J.H. Marburger. Relaxation Oscillations in Stimulated Brillouin Scattering. *Phys. Rev. A*, 4:1175–1182, September 1971.

16. I. Bar-Joseph, A.A. Friesem, E. Lichtman, and R.G. Waarts. Steady and Relaxation Oscillations of Stimulated Brillouin Scattering in Single-Mode Optical Fibers. *J. Opt. Soc. Am. B*, 2:1606–1611, October 1985.

17. W. Lu and R.G. Harrison. Origin of Chaotic Dynamics in Stimulated Brillouin Scattering. Submitted to Phys. Rev. Lett. May 1990.

18. B.Ya. Zel'dovich, N.F. Pilipetskii, and V.V. Shkunov. Phase Conjugation in Stimulated Scattering. *Sov. Phys. Usp.*, 25:713–737, October 1982.

19. B.Ya. Zel'dovich, N.F. Pilipetskii, and V.V. Shkunov. Chapter 6, Experimental Investigation of Wave-Front Reversal Under Stimulated Scattering. In *Optical Phase Conjugation* , edited by Robert A. Fisher, pages 135–167. Academic Press, Inc., New York, 1983.

20. B.Ya. Zel'dovich, V.I. Popovichev, V.V. Ragul'skii, and F.S. Faizullov. Connection Between the Wave Fronts of the Reflected and Exciting Light in Stimulated Mandel'shtam–Brillouin Scattering. *JETP Lett.*, pages 109–113, February 1972.

21. V. Wang and C.R. Guiliano. Correction of Phase Aberrations Via Stimulated Brillouin Scattering. *Opt. Lett.*, 2:4–6, January 1978.

22. R.C. Lind and C.R. Giuliano. Detailed Measurements of the Degree of Phase Conjugation by SBS. *Conference on Laser Engineering and Applications, CLEA '79*, pages 71–72, 1979.

23. R. Mays, Jr. and R.J. Lysiak. Phase Conjugated Wavefronts By Stimulated Brillouin and Raman Scattering. *Opt. Commun.*, 31:89–92, October 1979.

24. R. Mays, Jr. and R.J. Lysiak. Observations of Wavefront Reproduction By Stimulated Brillouin and Raman Scattering as a Function of Pump Power and Waveguide Dimensions. *Opt. Commun.*, 32:334–338, February 1980.

25. E.P. Ippen and R.H. Stolen. Stimulated Brillouin Scattering in Optical Fibers. *Appl. Phys. Lett.*, 21:539–541, December 1972.

26. K.O. Hill, B.S. Kawasaki, and D.C. Johnson. CW Brillouin Laser. *Appl. Phys. Lett.*, 28:608, May 1976.

27. K.O. Hill, D.C. Johnson, and B.S. Kawasaki. CW Generation of Multiple Stokes and Anti-Stokes Brillouin-Shifted Frequencies. *Appl. Phys. Lett.*, 29:185–187, August 1976.

28. Robert W. Boyd, A.L. Gaeta, R. Petrozzo, and K. Rzazewski. Initiation of Stimulated Brillouin Scattering By Quantum and Thermal Noise. *Tech. Digest,* Ann. Meet. Opt. Soc. Am., Paper TUA1, 69, October 1989.

29. R.H. Stolen. Polarization Effects in Fiber Raman and Brillouin Lasers. *IEEE J. Quantum Electron.*, 15:1157–1160, October 1979.

30. N. Uesugi, M. Ikeda, and Y. Sasaki. Maximum Single Frequency Input Power in a Long Optical Fibre Determined By Stimulated Brillouin Scattering. *Electron. Lett.*, 17:379–380, May 1981.

31. D. Cotter. Observation of Stimulated Brillouin Scattering in Low-Loss Silica Fibre at 1.3 Micron. *Electron. Lett.*, 18:495–496, June 1982.

32. Y. Aoki, K. Tajima, and I. Mito. Observation of Stimulated Brillouin Scattering in Single-Mode Fibres with Single-Frequency Laser-Diode Pumping. *Opt. Quantum Electron.*, 19:141–143, 1987.

33. R.G. Harrison, J.S. Uppal, A. Johnstone, and J.V. Moloney. Evidence of Chaotic Stimulated Brillouin Scattering in Optical Fibers. *Phys. Rev. Lett.*, 65:167–170, July 1990.

34. 1990. Compiled by K. Wink.

35. A. Bolle, G. Grosso, and B. Daino. Brillouin Gain Curve Dependence on Frequency Spectrum of PSK Modulated Signals. *Electron. Lett*, 25:2–3, January 1989.

36. Y. Aoki and K. Tajima. Dependence of the Stimulated Brillouin Scattering Threshold in Single-Mode Fibers on the Number of Longitudinal Modes of a Pump Laser. In *Tech. Digest, Conference on Lasers and Electro-Optics, CLEO '87,* Paper TUHH5, Baltimore, pages 86–87, 1987.

37. Y. Aoki, S. Kishida, and K. Washio. Stable CW Backward Raman Amplification in Optical Fibers by Stimulated Brillouin Scattering Suppression. *Appl. Opt.*, 25:1056–1060, April 1986.

38. J. Pelous and R. Vacher. Thermal Brillouin Scattering Measurements of the Attenuation of Longitudinal Hypersounds in Fused Quartz from 77 to 300 K. *Solid State Commun.*, 16:279–283, 1975.

39. N. Shibata, R. Waarts, and R. Braun. Brillouin-Gain Spectra for Single-Mode Fibers Having Pure-Silica, GeO_2-Doped, and P_2O_5-Doped Cores. *Opt. Lett.*, 12:269–271, April 1987.

40. Y. Azuma, N. Shibata, T. Horiguchi, and M. Tateda. Wavelength Dependence of Brillouin-Gain Spectra for Single-Mode Optical Fibers. *Elect. Lett.*, 24:250–252, March 1988.

41. N. Shibata, K. Okamoto, and Y. Azuma. Longitudinal Acoustic Modes and Brillouin-Gain Spectra for GeO_2-Doped-Core Single-Mode Fibers. *J. Opt. Soc. Am. B*, 6:1167–1174, June 1989.

42. R.H. Stolen, E.P. Ippen, and A.R. Tynes. Raman Oscillation in Glass Optical Waveguide. *Appl. Phys. Lett.*, 20:62–64, January 1972.

43. G.H. Sigel, Jr. Fiber Transmission Losses in High-Radiation Fields. *Proc. of the IEEE*, 68:1236–1240, October 1980.

44. R.M. Herman and M.A. Gray. Theoretical Prediction of the Stimulated Thermal Rayleigh Scattering in Liquids. *Phys. Rev. Lett.*, 19:824–828, October 1967.

45. M. Denariez and G. Bret. Investigation of Rayleigh Wings and Brilouin-Stimulated Scattering in Liquids. *Phys. Rev.*, 171:160–171, July 1968.

46. D. Marcuse. Theory of Dielectric Optical Waveguides. In *Quantum Electronics — Principles and Applications,* edited by Y. Pao. Academic Press, New York, 1974.

SECURITY CLASSIFICATION OF THIS PAGE

REPORT DOCUMENTATION PAGE

Form Approved
OMB No. 0704-0188

1a. REPORT SECURITY CLASSIFICATION UNCLASSIFIED	1b. RESTRICTIVE MARKINGS
2a. SECURITY CLASSIFICATION AUTHORITY	3. DISTRIBUTION/AVAILABILITY OF REPORT Approved for public release; distribution unlimited.
2b. DECLASSIFICATION/DOWNGRADING SCHEDULE	
4. PERFORMING ORGANIZATION REPORT NUMBER(S) AFIT/GEP/ENP/90S-1	5. MONITORING ORGANIZATION REPORT NUMBER(S)
6a. NAME OF PERFORMING ORGANIZATION School of Engineering 6b. OFFICE SYMBOL (If applicable)	7a. NAME OF MONITORING ORGANIZATION
6c. ADDRESS (City, State, and ZIP Code) Air Force Institute of Technology Wright-Patterson AFB OH 45433-5583	7b. ADDRESS (City, State, and ZIP Code)
8a. NAME OF FUNDING/SPONSORING ORGANIZATION 8b. OFFICE SYMBOL (If applicable)	9. PROCUREMENT INSTRUMENT IDENTIFICATION NUMBER
8c. ADDRESS (City, State, and ZIP Code)	10. SOURCE OF FUNDING NUMBERS PROGRAM ELEMENT NO. / PROJECT NO. / TASK NO / WORK UNIT ACCESSION NO.

11. TITLE (Include Security Classification)
OPTICAL PHASE CONJUGATION VIA STIMULATED BRILLOUIN SCATTERING IN MULTIMODE OPTICAL FIBER

12. PERSONAL AUTHOR(S)
Patrick T. Ryan, B.S. 1LT, USAF

13a. TYPE OF REPORT	13b. TIME COVERED	14. DATE OF REPORT (Year, Month, Day)	15. PAGE COUNT
MS Thesis	FROM _____ TO _____	1990 September	68

16. SUPPLEMENTARY NOTATION

17. COSATI CODES			18. SUBJECT TERMS (Continue on reverse if necessary and identify by block number)
FIELD	GROUP	SUB-GROUP	Phase Conjugation, Optical Fiber, Laser Beams, Stimulated Brillouin Scattering, Coupling (Interaction)
20	06	01	
09	06		

19. ABSTRACT (Continue on reverse if necessary and identify by block number)

The main objective of this thesis was to obtain phase conjugation of a laser beam using the process of stimulated Brillouin scattering (SBS) in optical fiber and to characterize the parameters involved. SBS in fiber is used for several reasons: high conversion efficiency, nanosecond response time, only the signal beam is required and fiber has a lower SBS threshold and superior power handling capabilities compared to either crystals or liquids. SBS theory is briefly described along with some results from previous work. Experimental results show the multimode fiber losses at coupled powers below about 2 W to be 16.4 ± 0.3 dB/km at 514.5 nm. The transmitted and backscattered power exhibited behavior similar to that previously reported for single-mode fiber. The SBS threshold power increased for shorter fibers and when index matching liquid was used. The Stokes shift was 32.78 ± 0.02 GHz and the measured gain coefficient was 10.2 times 10(-9) cm/W with an error of 10%. Most importantly, nonlinear optical phase conjugation was demonstrated for the first time. The polarization state of the pump beam was not reproduced, however. In addition, the SBS power exhibited bursts of strong fluctuations. — RH 47

20. DISTRIBUTION/AVAILABILITY OF ABSTRACT	21. ABSTRACT SECURITY CLASSIFICATION
☒ UNCLASSIFIED/UNLIMITED ☐ SAME AS RPT. ☐ DTIC USERS	UNCLASSIFIED

22a. NAME OF RESPONSIBLE INDIVIDUAL	22b. TELEPHONE (Include Area Code)	22c. OFFICE SYMBOL
Won B. Roh, Professor, AFIT	(513) 255-4498	AFIT/ENP

DD Form 1473, JUN 86 — Previous editions are obsolete. — SECURITY CLASSIFICATION OF THIS PAGE